



This discussion paper is/has been under review for the journal Geoscientific Model Development (GMD). Please refer to the corresponding final paper in GMD if available.

ModelE2-TOMAS development and evaluation using aerosol optical depths, mass and number concentrations

Y. H. Lee¹, P. J. Adams², and D. T. Shindell³

¹NASA Goddard Institute for Space Studies and Columbia Earth Institute, New York, NY, USA

²Department of Civil and Environmental Engineering and Department of Engineering Public Policy, Carnegie Mellon University, Pittsburgh, PA, USA

³Earth and Ocean Sciences, Nicholas School of the Environment, Duke University, Durham, NC 27708, USA

Received: 11 July 2014 – Accepted: 5 August 2014 – Published: 3 September 2014

Correspondence to: Y. H. Lee (yunha.lee.00@gmail.com)

Published by Copernicus Publications on behalf of the European Geosciences Union.

GMDD

7, 5831–5918, 2014

ModelE2-TOMAS:
global aerosol
microphysics model

Y. H. Lee et al.

Title Page

Abstract

Introduction

Conclusions

References

Tables

Figures



Back

Close

Full Screen / Esc

Printer-friendly Version

Interactive Discussion



Abstract

The Two-Moment Aerosol Sectional microphysics model (TOMAS) has been integrated into the state-of-the-art general circulation model, GISS ModelE2. TOMAS has the flexibility to select a size resolution as well as the lower size cutoff. A computationally efficient version of TOMAS is used here, which has 15 size bins covering 3 nm to 10 μm aerosol dry diameter. For each bin, it simulates the total aerosol number concentration and mass concentrations of sulphate, pure elementary carbon (hydrophobic), mixed elemental carbon (hydrophilic), hydrophobic organic matter, hydrophilic organic matter, sea salt, mineral dust, ammonium, and aerosol-associated water. This paper provides a detailed description of the ModelE2-TOMAS model and evaluates the model against various observations including aerosol precursor gas concentrations, aerosol mass and number concentrations, and aerosol optical depths. Additionally, global budgets in ModelE2-TOMAS are compared with those of other global aerosol models, and the TOMAS model is compared to the default aerosol model in ModelE2, which is a bulk aerosol model. Overall, the ModelE2-TOMAS predictions are within the range of other global aerosol model predictions, and the model has a reasonable agreement with observations of sulphur species and other aerosol components as well as aerosol optical depth. However, ModelE2-TOMAS (as well as the bulk aerosol model) cannot capture the observed vertical distribution of sulphur dioxide over the Pacific Ocean possibly due to overly strong convective transport. The TOMAS model successfully captures observed aerosol number concentrations and cloud condensation nuclei concentrations. Anthropogenic aerosol burdens in the bulk aerosol model running in the same host model as TOMAS (ModelE2) differ by a few percent to a factor of 2 regionally, mainly due to differences in aerosol processes including deposition, cloud processing, and emission parameterizations. Larger differences are found for naturally emitted aerosols such as sea salt and mineral dust. With TOMAS, ModelE2 has three different aerosol models (the bulk aerosol model and modal-based aerosol microphysics model,

ModelE2-TOMAS: global aerosol microphysics model

Y. H. Lee et al.

[Title Page](#)

[Abstract](#)

[Introduction](#)

[Conclusions](#)

[References](#)

[Tables](#)

[Figures](#)



[Back](#)

[Close](#)

[Full Screen / Esc](#)

[Printer-friendly Version](#)

[Interactive Discussion](#)



1 Introduction

Aerosols perturb the energy balance of the Earth–atmosphere system by scattering and absorbing solar and terrestrial radiation, known as the aerosol direct effect, and by modifying cloud properties such as via acting as cloud condensation nuclei (CCN), known as aerosol indirect effects (e.g. Lohmann and Feichter, 2005; Forster and Ramaswamy, 2007). The recently published IPCC AR5 (Intergovernmental Panel on Climate Change Fifth Assessment Report) refers to these as aerosol-radiation interactions and aerosol-cloud interactions, respectively (Boucher et al., 2013). For light-absorbing aerosols such as black carbon and mineral dust, the ambient air can be heated as a result of their direct effect, affecting relative humidity and atmospheric stability, which is known as the semi-direct effect. The largest uncertainty in estimating anthropogenic climate forcing is from the aerosol indirect effects (Myhre et al., 2013b). Since it is not easily estimated from observations due to natural variability in cloud properties and the lack of observations of the pre-industrial atmosphere, estimates of aerosol indirect effects have been mainly based on general circulation models (GCMs). Thus, there have been growing efforts to develop and improve aerosol microphysics models for a more physically based representation of atmospheric aerosol number and CCN concentrations (e.g. Adams and Seinfeld, 2002; Easter et al., 2004; Vignati et al., 2004; Lauer et al., 2005; Liu et al., 2005; Spracklen et al., 2005; Stier et al., 2005; Bauer et al., 2008; Trivitayanurak et al., 2008; Yu and Luo, 2009; Mann et al., 2010; Lee and Adams, 2012).

Aerosol microphysics models can be broadly categorized into moment, modal, and sectional methods, depending on how they represent the aerosol size distribution. In general, moment-based methods track lower-order (radial) moments of a size distribution, and modal-based methods use an analytical function (e.g. a lognormal

Title Page	
Abstract	Introduction
Conclusions	References
Tables	Figures
	
	
Full Screen / Esc	
Printer-friendly Version	
Interactive Discussion	



distribution) to represent a mode of the particle population. Sectional methods represent a size distribution by predicting the amount of aerosols in several size sections or “bins”. Even though we generally classify aerosol microphysics models into the three categories, some aerosol microphysics models are hybrid of two methods. For example, the TOMAS aerosol microphysics model is mostly a sectional scheme but mixed with a moment-based scheme.

Sectional methods can be divided into single-moment sectional methods that typically track either aerosol number or mass in each bin and two-moment sectional methods that explicitly track both aerosol number (i.e. zeroth moment) and mass (i.e. 1st mass moment) in each size section. Unlike single-moment sectional approaches, two-moment sectional methods can conserve both number and mass very accurately (Tzivion et al., 1987, 2001; Adams and Seinfeld, 2002; Jung et al., 2006) but have a high computational burden. The modal and the moment-based approaches are generally more computationally efficient but may not represent abrupt transitions in a size distribution well, which can occur during cloud processing (Zhang et al., 1999).

The TOMAS aerosol microphysics model (Adams and Seinfeld, 2002; Tzivion et al., 1987, 1989) has been developed to study tropospheric aerosol microphysics and predict cloud condensation nuclei (CCN) concentrations. The TOMAS model has been previously implemented into the climate model of Goddard Institute for Space Studies General Circulation Model II-prime (GISS GCM II-prime), referred to as “GISS-TOMAS” (Lee and Adams, 2010). It has also been incorporated into GEOS-CHEM (Trivitayanurak et al., 2008), the regional model PMCAMx-UF (Jung et al., 2010), and the Large-Eddy Simulation model (Stevens et al., 2012; Singh et al., 2014). The GISS GCM II-prime has horizontal grid dimensions of 4° latitude and 5° longitude, with nine vertical sigma layers between the surface to the 10 hPa level (Hansen et al., 1983). Modules for each of the major aerosol species have been developed for the GISS GCM II-prime, and the GISS-TOMAS model has been evaluated with ground-level measurements such as number and mass concentrations, deposition fluxes, and remote sensing observations (Adams and Seinfeld, 2002; Pierce and Adams, 2006; Pierce et al., 2007;

[Title Page](#)[Abstract](#)[Introduction](#)[Conclusions](#)[References](#)[Tables](#)[Figures](#)[◀](#)[▶](#)[◀](#)[▶](#)[Back](#)[Close](#)[Full Screen / Esc](#)[Printer-friendly Version](#)[Interactive Discussion](#)

Lee et al., 2009; Lee and Adams, 2010). Despite the accuracy in predicting aerosol microphysical process in TOMAS, the heavy computational burden of the original TOMAS model in a GCM became an obstacle to study aerosol indirect effects that typically requires multi-year simulations. Lee and Adams (2012) developed more computationally efficient versions of the TOMAS model (Fast TOMAS), which are 2–3 times faster than the original TOMAS model with only a few percent increases in microphysical errors. However, a remaining weakness for the GISS-TOMAS model is the outdated host model, the GISS GCM II-prime.

Since uncertainties in the estimates of aerosol forcing come from not only aerosol modelling itself but also other parts of the host GCM (e.g., cloud physics, planetary boundary layer, and advection), it is important to include the improvements in both aerosol modelling and the other parts of GCM. Therefore, here we incorporate the TOMAS model into the new version of GISS GCM (i.e., ModelE2), referred to as “ModelE2-TOMAS”. ModelE2 now has three different aerosol models available: modelE2-TOMAS, a bulk aerosol model (e.g. Koch et al., 2006) that has no micro-physics, and the modal-based aerosol microphysics module, MATRIX (Multiconfiguration Aerosol TRacker of mIXing state) (Bauer et al., 2008). The combination of several aerosol models into the same host GCM allows ModelE2 to explore the uncertainties in predicting aerosol characteristics and their climate effects that are associated with aerosol modelling (e.g. different numerical approaches) in the same host model.

ModelE2-TOMAS has been used in several recent studies under the Atmospheric Chemistry and Climate Model Intercomparison Project (ACCMIP) that has a goal of understanding composition changes and the associated radiative forcing between 1850 and 2100 (Bowman et al., 2013; Lamarque et al., 2013a, b; Lee et al., 2013a; Nabat et al., 2013; Naik et al., 2013; Shindell et al., 2013; Stevenson et al., 2013; Young et al., 2013). The model description was very brief in these papers, so the major goal of this paper is to describe the ModelE2-TOMAS model and to evaluate against observations of aerosol mass and number as well as aerosol optical depth. Aerosol direct and indirect forcings using ModelE2-TOMAS will be discussed in a separate paper. In this

Title Page	
Abstract	Introduction
Conclusions	References
Tables	Figures
◀	▶
◀	▶
Back	Close
Full Screen / Esc	
Printer-friendly Version	
Interactive Discussion	



paper, as a comparison with TOMAS, we include the bulk aerosol model in ModelE2, which has been used as the default aerosol model in various GISS GCM simulations, including GISS' Coupled Model Intercomparison Project Phase 5 (CMIP5) simulations (e.g., Schmidt et al., 2014). Section 2 provides the basic description of ModelE2 including the bulk aerosol model, and Sect. 3, the description of the TOMAS aerosol microphysics model. Section 4 explains the emissions and design of simulations. Section 5 presents the global budgets of the simulated aerosols and the evaluation of the TOMAS and bulk aerosol model in ModelE2 against observations of aerosol mass concentrations and aerosol optical depth and the evaluation of the TOMAS number predictions against observations. Conclusions follow in Sect. 6.

2 GISS GCM ModelE2

The newest version of the GISS climate model used in this study is called ModelE2 and was used to perform CMIP5 simulations in support of IPCC AR5. The model physics are mostly similar to GISS ModelE (CMIP3 version: Schmidt et al., 2006), and the updates made in ModelE2 are discussed in Schmidt et al. (2014). A brief description of ModelE2 is given here. The model has 2° latitude by 2.5° longitude resolution, with 40 vertical hybrid sigma layers from the surface to 0.1 hPa (80 km). Tracers, heat, and humidity are advected using the highly nondiffusive Quadratic Upstream Scheme (Prather, 1986). The radiation scheme accounts for size-dependent scattering properties of clouds and aerosols based on Mie scattering (Hansen et al., 1983) and non-spherical light scattering of cirrus and dust particles based on T-matrix theory (Mishchenko et al., 1996). It also includes the impact of water uptake by hydroscopic species on their radiative properties. The model uses moist convective and large-scale stratiform clouds parameterizations that are similar to Del Genio (1993) and Del Genio et al. (1996) but have been improved in several respects (see details in Schmidt et al., 2006, 2014). The physics timestep is 30 min, and the radiation is calculated every 2.5 h.

ModelE2-TOMAS:
global aerosol
microphysics model

Y. H. Lee et al.

[Title Page](#)

[Abstract](#)

[Introduction](#)

[Conclusions](#)

[References](#)

[Tables](#)

[Figures](#)



[Back](#)

[Close](#)

[Full Screen / Esc](#)

[Printer-friendly Version](#)

[Interactive Discussion](#)



2.1 Bulk aerosol model

ModelE2 includes a default aerosol module that has no microphysics (thus, referred to as the bulk aerosol model). The bulk aerosol model has sulphate (Koch et al., 2006, 2007, 2011), carbonaceous aerosols (Koch et al., 2007), secondary organic aerosols (Tsigaridis and Kanakidou, 2007), sea salt (Koch et al., 2006; Tsigaridis et al., 2013), dust (Miller et al., 2006), and nitrate (Bauer et al., 2007). Along with sulphate, the model also predicts sulphur dioxide, dimethyl sulfide (DMS) and methanesulfonic acid (MSA) (Koch et al., 2006). Sea salt particles have two size classes with a fine mode ($0.1\text{ }\mu\text{m}$ to $1\text{ }\mu\text{m}$ in dry radii) and a coarse mode ($1\text{ }\mu\text{m}$ to $4\text{ }\mu\text{m}$ in dry radii). Dust particles have four size classes with radii between $0.1\text{--}1\text{ }\mu\text{m}$ (clay), $1\text{--}2\text{ }\mu\text{m}$ (silt1), $2\text{--}4\text{ }\mu\text{m}$ (silt2), and $4\text{--}8\text{ }\mu\text{m}$ (silt3). The model accounts for heterogeneous chemistry on mineral dust particle surfaces to form nitrate and sulphate (Bauer and Koch, 2005).

In ModelE2, the surface boundary conditions are defined using dry deposition and interactive surface sources (Koch et al., 2006). The dry deposition scheme is tightly coupled to the model boundary layer process and is based on a resistance-in-series scheme derived from the Harvard GISS-CTM, which is applied between the surface layer (10 m) and the ground (Koch et al., 2006). Wet deposition is determined by several processes including rainout within clouds, washout below precipitating regions, scavenging within and below cloud updrafts, evaporation of falling precipitation, transport along with convective plumes, and detrainment and evaporation from convective plumes (Koch et al., 2006; Shindell et al., 2006). ModelE2 includes a dissolved species budget scheme for stratiform clouds, which has an impact on sulphate formation via aqueous oxidations, since some sulphate formed in clouds undergoes wet scavenging instead of being added back to the sulphate in air (Koch et al., 2006).

Tropospheric/stratospheric chemistry in ModelE2 includes 156 chemical reactions among 51 gas species (Shindell et al., 2013). In ModelE2, chemistry and aerosols are fully interactive, so that the oxidation fields used for sulphate formation are from the chemistry model (not prescribed) and the photolysis rates are affected by light

[Title Page](#)[Abstract](#)[Introduction](#)[Conclusions](#)[References](#)[Tables](#)[Figures](#)[◀](#)[▶](#)[◀](#)[▶](#)[Back](#)[Close](#)[Full Screen / Esc](#)[Printer-friendly Version](#)[Interactive Discussion](#)

attenuation by aerosols (Shindell et al., 2013). Photolysis rates are computed using the Fast-J2 scheme (Bian and Prather, 2002). Aerosol indirect effects are based on an empirical parameterization (2002; Menon et al., 2008).

3 TOMAS aerosol microphysics model

- 5 The TOMAS aerosol microphysics model uses a sectional approach that represents the aerosol size distribution by predicting the amount of aerosol in several size categories or “bins”. TOMAS tracks two moments of the aerosol size distribution in each size bin: total aerosol number (i.e., 0th moment) and mass (i.e., 1st mass moment). Total mass is decomposed into several aerosol species, allowing prediction of the size-
10 resolved aerosol composition. In total, the TOMAS model tracks ten quantities for each size bin: sulphate mass, sea-salt mass, mass of pure (hydrophobic) elemental carbon (EC), mass of mixed (aged) EC, mass of hydrophobic organic matter (OM), mass of hydrophilic OM, mass of mineral dust, mass of ammonium, mass of water and the number of aerosol particles in that bin; the ammonium mass is diagnosed in each
15 size bin based on sulphate mass within the TOMAS model but is a single bulk tracer for purposes of model processes outside TOMAS (e.g. advection and deposition). In addition, the model tracks one bulk aerosol-phase species, ammonium (NH_4), and four bulk gas-phase species: sulphur dioxide (SO_2), dimethylsulfide (DMS), sulphuric acid (H_2SO_4), and a lumped gas-phase tracer that represents oxidized organic vapors
20 forming secondary organic aerosol (SOA). The gas-phase H_2SO_4 is assumed to be in pseudo-steady state equilibrium between its chemical production and condensational/nucleation losses (Pierce and Adams, 2009b). TOMAS uses a moving sectional approach to treat water uptake; changes in water mass do not move particles between sections. Water uptake by sulphate, sea salt, and hydrophilic OM is accounted for in
25 the model. Detailed descriptions of the TOMAS microphysics scheme can be found in Adams and Seinfeld (2002), Lee and Adams (2012), and Lee et al. (2013b).

Title Page	
Abstract	Introduction
Conclusions	References
Tables	Figures
◀◀	▶▶
◀	▶
Back	Close
Full Screen / Esc	
Printer-friendly Version	
Interactive Discussion	



Several nucleation schemes are available in TOMAS, including binary nucleation (Vehkamaki et al., 2002), ternary nucleation (Napari et al., 2002), ion-induced nucleation (Modgil et al., 2005), and activation nucleation with an A factor of $2 \times 10^{-6} \text{ s}^{-1}$ (Sihto et al., 2006) for the boundary layer (\sim up to 900 mbar). For the simulations used in this paper, only binary nucleation is used.

With the development of computationally efficient TOMAS models (i.e. Fast TOMAS), the TOMAS microphysics module became more flexible in term of varying particle size resolution, i.e. the number of size bins (Lee and Adams, 2012). For the size range of 10 nm to 10 μm , the original TOMAS uses 30 bins, and the Fast TOMAS uses 15 bins or 12 bins, which reduces the computational burden by 2–3 times compared to the original TOMAS. The lower size cutoff in TOMAS can also vary from 10 nm to 3 nm or from 10 nm to 1 nm (Lee et al., 2013b). Among several possible configurations, ModelE2-TOMAS currently uses either 12 bins covering 10 nm to 10 μm or 15 bins covering 3 nm to 10 μm , which is the most computationally efficient version of TOMAS for the given size range; for the 12 bins case, the first ten size bins cover from 10 nm to 1 μm and the last two bins from 1 μm to 10 μm ; for the 15 bins cases, it is the same as the 12 bins from 10 nm to 10 μm , and the additional three bins are assigned from 3 nm to 10 nm. More configurations will be available in the near future. In this paper, we used TOMAS with 15 bins covering 3 nm to 10 μm .

The wet deposition scheme in ModelE2-TOMAS is identical to the one used in ModelE2 except for the following. First, the TOMAS model condenses the sulphuric acid formed from aqueous oxidation by hydrogen peroxide (H_2O_2) directly onto sulphate aerosols in ambient air rather than maintaining a separate tracer for dissolved sulphate. Compared to the bulk aerosol model, this is a simplification because the sulphate formed from aqueous oxidation should release to the air only when the cloud water evaporates. It is adopted here for simplicity but will be improved in the future. The other difference is that the wet/dry deposition in the TOMAS model accounts for particle size dependence. For in-cloud scavenging, modified Köhler theory is used to obtain the critical supersaturation for activation of each size section and to determine which particles

ModelE2-TOMAS: global aerosol microphysics model

Y. H. Lee et al.

[Title Page](#)

[Abstract](#)

[Introduction](#)

[Conclusions](#)

[References](#)

[Tables](#)

[Figures](#)

◀

▶

◀

▶

[Back](#)

[Close](#)

[Full Screen / Esc](#)

[Printer-friendly Version](#)

[Interactive Discussion](#)



Title Page	
Abstract	Introduction
Conclusions	References
Tables	Figures
◀	▶
◀	▶
Back	Close
Full Screen / Esc	
Printer-friendly Version	
Interactive Discussion	

activate and are subject to in-cloud (nucleation) scavenging (Pierce et al., 2007). The fraction of activated aerosols removed by wet deposition is proportional to the fraction of cloud water that precipitates. For in-cloud scavenging, the large-scale and convective clouds in the model are assumed to have a supersaturation of 0.2 %; unlike GISS-TOMAS that used a supersaturation of 1.0 % for convective clouds, a supersaturation of 0.2 % is assumed in ModelE2-TOMAS in order to capture the observed hopple gap (~ 100 nm) in the marine boundary layer. For below-cloud scavenging, a first-order removal scheme implemented for bulk aerosols by Koch et al. (1999) is modified for size-resolved aerosols (Adams and Seinfeld, 2002). In cloud processes such as activation and wet deposition, aerosols are treated as externally mixed or pure populations. Dry deposition is identical to the existing resistance-in-series scheme in ModelE2, but the ModelE2-TOMAS model treats a size-dependent gravitational settling of particles and a size-dependent resistance in the quasi-laminar sublayer (Seinfeld and Pandis, 1998; Adams and Seinfeld, 2002).

4 Simulation setup

4.1 Emissions

The emissions used in this study are summarized in Table 1. The simulations used 2000 emissions from the anthropogenic emissions inventory created for CMIP5 (Lamarque et al., 2013b) and climatologically averaged biomass burning emissions from GFED3 for 1997 to 2009 (van der Werf et al., 2010). For SO_2 , in addition to the anthropogenic emissions, continuous volcanic emissions from GEIA (Global Emissions Initiative) are used but increased by a factor of 1.5 as in the AEROCOM intercomparison emissions in Dentener et al. (2006). Sea-salt emission is based on Gong (2003), which extends the lower size limit of the Monahan et al. (1986) emission from $0.4 \mu\text{m}$ to $0.02 \mu\text{m}$. Dust emission is based on the source distribution from Ginoux et al. (2001) and is proportional to the third power of the wind speed (at 10 m in height) above

Title Page	
Abstract	Introduction
Conclusions	References
Tables	Figures
◀	▶
◀	▶
Back	Close
Full Screen / Esc	
Printer-friendly Version	
Interactive Discussion	

a threshold that is a function of soil moisture. Subgrid-variation of the wind speed in a GCM grid box, which is created by boundary-layer turbulence and dry/wet convection, is accounted for the modeled dust emissions (Cakmur et al., 2006; Miller et al., 2006). DMS emission is based on the seawater DMS concentrations of Kettle et al. (1999).

5 For the sea-to-air transfer function used in the DMS emissions, TOMAS runs are based on Liss and Merlivat (1986), and the bulk aerosol model run is based on Nightingale et al. (2000).

Nightingale et al. (2000) provides a revised parameterization based on observations of the sea-to-air transfer rate scatter between two classical parameterizations (i.e., Liss

10 and Merlivat, 1986; Wanninkhof, 1992), and it has been more favoured in many global DMS models than the two classical parameterizations. However, DMS emission is quite uncertain. Estimates of the global DMS emissions range from 16 to 54 Tg S yr⁻¹ (Kettle and Andreae, 2000), depending on the choice of DMS sea surface climatology, sea-to-air transfer rate parameterization, and wind speed data. DMS emission rates

15 from TOMAS and the bulk aerosol model are within the range. The Liss and Merlivat (1986) parameterization is used in TOMAS, because a ModelE2-TOMAS run based on Nightingale et al. (2000) overpredicts the DMS and SO₂ concentrations over remote oceanic regions especially in the Southern Hemisphere. Koch et al. (2006) showed that the sea-to-air transfer function from Nightingale et al. (2000) increased annual

20 DMS emissions by roughly a factor of two compared to the emission based on Liss and Merlivat (1986). This was desirable in the bulk aerosol model because of the underprediction of sulphate in remote oceanic regions in that model, although the model DMS and MSA (oxidized from DMS) tended to be excessive in SH oceanic regions especially near Antarctica. However, despite the higher DMS emissions, it turned out that

25 the sulphate was still underpredicted because sulphate formed by aqueous oxidation was subject to wet scavenging before releasing to the ambient air as a result of the updated dissolved species budget scheme (Koch et al., 2006).

4.2 TOMAS run setup

We performed the simulations nudged with winds from the MERRA (Modern Era Retrospective-analysis for Research and Applications) reanalysis meteorological fields from 2000 to 2003 with 3 years spin-up (i.e., 1997–1999). Primary emission of particulate sulphate is assumed to be 1.0 % of total sulphur emissions. Emissions size distributions assumed for TOMAS are summarized in Table 2. Primary sulphate emission is assumed to have a bi-modal lognormal distribution that assigns 5 % of the primary sulphate emissions as a nucleation mode with a geometric number mean diameter (GMD) of 10 nm and a geometric standard deviation (GSD) of 1.6 and the rest as an Aitken mode with GMD of 70 nm and GSD of 2. For fossil fuel and biofuel emissions, the size of primary carbonaceous aerosol emissions is assumed to fit a lognormal size distribution with a GMD of 60 nm and a GSD of 1.59 for both EC and OM (Stier et al., 1995). For carbonaceous aerosols of biomass burning emissions, a lognormal size distribution is assumed to have a GMD of 150 nm and a GSD of 1.59. Note that an emission size distribution used for the biofuel emissions is generally the same as that for biomass burning emissions as their burning materials are the same (e.g. Dentener et al., 2006), but our model assumes the biofuel emission size distributions follow the fossil fuel because the CMIP5 emissions does not provide a separate category for biofuel emissions (e.g. biofuel used for cooking and heating are assigned as the residential sector, which also includes fossil fuel usage). The OC (organic carbon) : OM (organic matter) ratio is assumed to be 1 : 1.4.

ModelE2-TOMAS assumes larger particles for sulphate and carbonaceous aerosols than GISS-TOMAS (Lee et al., 2013) to capture the observed aerosol number concentrations better. This is very likely due to the following: (1) GISS-TOMAS attributed the primary sulphate emissions only to anthropogenic sulphur emissions (excluding biomass burning emissions), while ModelE2-TOMAS attributes these to all sulphur emissions, (2) GISS-TOMAS applied the biomass-burning emission size distributions of carbonaceous aerosols to the biofuel emissions, which is coarser than the fossil fuel

GMDD

7, 5831–5918, 2014

ModelE2-TOMAS:
global aerosol
microphysics model

Y. H. Lee et al.

[Title Page](#)

[Abstract](#)

[Introduction](#)

[Conclusions](#)

[References](#)

[Tables](#)

[Figures](#)

◀

▶

◀

▶

[Back](#)

[Close](#)

[Full Screen / Esc](#)

[Printer-friendly Version](#)

[Interactive Discussion](#)



emission size distribution. Whereas the GISS-TOMAS does not apply primary sulphate for biomass burning and volcanic emissions, ModelE2-TOMAS does. Additionally the emission size distributions used for biomass burning and volcanic emissions are finer than the AEROCOM recommendations in Dentener et al. (2006). However, the model number concentrations and size distributions are changed little when applying the AEROCOM recommended emission distributions (not shown). Note that the biomass burning and volcanic emissions for sulphur are 1.4 Tg Syr^{-1} and 12.5 Tg Syr^{-1} , respectively.

Following the soil size assumptions used in GISS-TOMAS (Lee et al., 2009), the clay distribution is assumed to have a GMD of $0.14 \mu\text{m}$ and a GSD of 2, and the silt distribution, a GMD of $1.15 \mu\text{m}$ and a GSD of 2. Using this distribution, fifteen percent of the silt emissions flux falls out of the upper size cutoff (i.e., $10 \mu\text{m}$), and thus they are excluded.

Compared to the run setup described above (hereafter, referred to as the “BASE” run), we additionally ran two other sensitivity runs with the TOMAS model by perturbing the nucleation process to evaluate changes in number concentrations (Table 1). The first sensitivity run is called “NoNUC”, in which we turned off nucleation to estimate the contribution of primary emissions to aerosol number concentrations. The other run is called “LowNUC”, in which we reduced the nucleation rate by using 5 times lower sulphuric acid concentrations to compute nucleation rates. Note that sulphuric acid concentrations are not perturbed in other processes, and the model sulphuric acid budget is little influenced by this treatment. The boundary-layer nucleation is off in all simulations because it tends to overpredict aerosol number concentrations in our model. Also we do not show any run with the ternary nucleation (Napari et al., 2002) because it overpredicts aerosol number concentration severely (not shown).

4.3 The bulk aerosol model run setup

To compare the TOMAS microphysics model with the default aerosol model in ModelE2 (i.e. the bulk aerosol model), we ran analogous simulation using the bulk aerosol

Title Page	
Abstract	Introduction
Conclusions	References
Tables	Figures
◀	▶
◀	▶
Back	Close
Full Screen / Esc	
Printer-friendly Version	
Interactive Discussion	



Title Page	
Abstract	Introduction
Conclusions	References
Tables	Figures
◀	▶
◀	▶
Back	Close
Full Screen / Esc	
Printer-friendly Version	
Interactive Discussion	

model with the MERRA reanalysis meteorological fields from 2000 to 2003 with 3 years spin-up. The natural emissions and emissions-relevant setup are not necessarily same between the bulk and TOMAS models. This is because we maintain the natural emissions/setup used in the bulk aerosol model, which has been chosen carefully in previous studies. Here, we note that the differences between the bulk aerosol model and TOMAS. First, as mentioned in Sect. 4.1, the bulk aerosol model uses the sea-to-air transfer function of Nightingale et al. (2000) instead of Liss and Merlivat (1986), because Koch et al. (2006) prefers the newer DMS emissions to improve a sulphate prediction in the remote marine locations. Second, the same sea salt and dust emission schemes are applied in both aerosol models, but different assumptions for the upper limit of particle size are used: 8 µm in diameter for sea salt and 16 µm in diameter for dust in the bulk aerosol model; 10 µm in TOMAS. Third, the bulk aerosol model assumes 2.5 % of the total sulphur as primary sulphate as followed by the AEROCOM study (Dentener et al., 2006). Aerosol number predictions are sensitive to the primary sulphate assumption, but sulphate mass concentrations are not. When using the 2.5 % assumption in ModelE2-TOMAS, we found that the simulated aerosol number concentrations were biased high, and the model size distribution predictions were also poor. Note that Pierce and Adams (2009a) shows that GISS-TOMAS also overpredicts aerosol number concentration with the 2.5 % assumptions.

5 Model results and evaluations

In this section, we present global-annual budgets, spatial distributions, and evaluations of the model aerosol precursor gases (in Sect. 5.1), aerosol mass (in Sects. 5.2 and 5.3), aerosol optical depths (AODs; in Sect. 5.4) and aerosol number (in Sects. 5.5 and 5.6). The observations used for model evaluations are from surface-based, aircraft-based and remote-sensing measurements. More details of the observations are provided in each subsection. To compare with the TOMAS results, we included the bulk aerosol model results in global-annual budgets and model evaluations. Only the BASE

run results are used in Sects. 5.1 to 5.4 because the predicted aerosol precursor gases concentrations, aerosol mass concentrations, and AODs from the nucleation sensitivity runs are quite similar to the BASE run.

Model skill is quantified in terms of log-mean normalized bias (LMNB) and log-mean normalized error (LMNE) when evaluating with annual-mean concentrations measurements and normalized mean bias (NMB) and correlation coefficient (R) when evaluating with an observed annual cycle and aerosol optical depth (both monthly and annually averaged AODs).

5.1 Aerosol precursor gases

Global budgets of DMS and SO_2 in ModelE2-TOMAS are presented in Table 3 with a range obtained from several global models including Wang et al. (2011), Liu et al. (2005), and those listed in Liu et al. (2005). The DMS and SO_2 budgets in ModelE2-TOMAS are within the ranges of the other global models. In case of the bulk aerosol model in ModelE2 (in Table 4), the global burden of DMS is about a factor of two higher than the TOMAS model because the DMS emission rate is $\sim 78\%$ higher by using the newer sea-to-air transfer functions by Nightingale et al. (2000). Despite the different DMS emissions and SO_2 emissions (due to the primary sulphate emission assumption, 1 % vs. 2.5 %), the global burden of SO_2 is quite similar to that in the ModelE2-TOMAS model. The dominant SO_2 removal processes are aqueous oxidation and dry deposition in both models.

When using the same DMS emissions in ModelE2-TOMAS as in the bulk aerosol model, the DMS global budgets are almost identical, but the SO_2 budgets vary substantially due to the differences in SO_2 modelling, i.e., heterogeneous SO_2 oxidation and photolysis (see Sect. 2). The heterogeneous sulphur dioxide oxidation on dust aerosol surfaces, which is only included in the bulk aerosol model, accounts for 25 % of the total gas-phase oxidation loss. Based on Bauer and Koch (2005), including the heterogeneous chemistry, global SO_2 burden can decrease 32 %, and global sulphate burden can increase 3 %. The simulated photolysis rates in the bulk aerosol model are

[Title Page](#)[Abstract](#)[Introduction](#)[Conclusions](#)[References](#)[Tables](#)[Figures](#)[◀](#)[▶](#)[◀](#)[▶](#)[Back](#)[Close](#)[Full Screen / Esc](#)[Printer-friendly Version](#)[Interactive Discussion](#)

ModelE2-TOMAS:
global aerosol
microphysics model

Y. H. Lee et al.

Title Page	
Abstract	Introduction
Conclusions	References
Tables	Figures
◀	▶
◀	▶
Back	Close
Full Screen / Esc	
Printer-friendly Version	
Interactive Discussion	



affected by aerosol optical depth, affecting hydroxide (OH) and other gas tracer concentrations – Naik et al. (2013) show a higher OH concentration in ModelE2-TOMAS than the bulk aerosol model. Overall, using the same DMS emissions in TOMAS results in a higher SO_2 burden and worse agreement for SO_2 and sulphate concentrations over remote oceanic regions (not shown).

The global budgets of H_2SO_4 and SOA precursor gas in the TOMAS model are not included in Table 3 but are summarized here. The simulated H_2SO_4 has a total source rate of $12.3 \text{ Tg S yr}^{-1}$, matching the SO_2 gas-phase oxidation, and is used in aerosol microphysics (i.e. 12 Tg yr^{-1} for condensation and 0.3 Tg yr^{-1} for nucleation). The model SOA precursor gas has a total source rate of 17.1 Tg yr^{-1} , assumed to be 10 % of the terpene emission, and is condensed as hydrophilic OM.

Figure 1 shows global maps of annual-mean DMS and SO_2 column mass concentrations. The spatial distribution of DMS concentrations is driven by its emission and OH and NO_3 concentrations, which oxidize DMS to form MSA and SO_2 . The model DMS concentrations are most pronounced in the Southern Ocean and the Northern Atlantic oceans due to high seawater DMS concentrations during summer. The simulated SO_2 concentration is very high over industrial regions due to the anthropogenic emissions and is also high over the Southern Ocean due to DMS oxidation. Several local hotspots of SO_2 shown in Fig. 1 are due to volcanic emissions.

Annually averaged surface-layer SO_2 concentrations from both TOMAS and the bulk aerosol models are evaluated against observations from the EMEP (European Monitoring and Evaluation Programme, <http://www.emep.int>) and CASTNET (Clean Air Status and Trends Network, <http://epa.gov/castnet/javaweb/index.html>) networks (see Fig. 2). We used 2000–2004 mean SO_2 measurements for the EMEP network and 1995–2005 mean SO_2 data for the CASTNET network. Performance of TOMAS and the bulk aerosol model for predicted SO_2 concentrations in these locations is almost the same (i.e. $\text{LMNB} = 0.25\text{--}0.26$ and $\text{LMNE} = 0.34$ for the EMEP network; $\text{LMNB} = 0.09$ and $\text{LMNE} = 0.29$ for the CASTNET network), and the continental SO_2 predictions agree with the observation on average roughly within a factor of two. The two aerosol models

ModelE2-TOMAS: global aerosol microphysics model

Y. H. Lee et al.

[Title Page](#)

[Abstract](#)

[Introduction](#)

[Conclusions](#)

[References](#)

[Tables](#)

[Figures](#)

◀

▶

◀

▶

[Back](#)

[Close](#)

[Full Screen / Esc](#)

[Printer-friendly Version](#)

[Interactive Discussion](#)



Title Page	
Abstract	Introduction
Conclusions	References
Tables	Figures
◀	▶
◀	▶
Back	Close
Full Screen / Esc	
Printer-friendly Version	
Interactive Discussion	



although the surface DMS is different as their emissions are not the same. Both models show good agreement with the observations (mostly within 25th and 75th percentile of observed values), especially capturing a strong concentration decrease from the surface to the free troposphere. Interestingly, the model DMS seems to show an increase above ~ 8 km quite consistently throughout the sites.

In the case of SO₂, even though the agreement is not as good as that seen for DMS, both aerosol models seem to capture the observed magnitude approximately within a factor of two. The overall vertical patterns shown in the models are frequently not in agreement with the observations. Generally, the observations show enhanced SO₂ concentrations in the boundary layer that the model does not capture. Considering the small DMS peak at 8 km and the elevated SO₂ in the upper/free troposphere in the models, this might indicate too strong vertical transport (at least over the Pacific Ocean) in the model. Although the elevated SO₂ mixing ratios might be due to too weak wet scavenging (including aqueous chemistry) of SO₂, we did not see any noticeable improvement when increasing SO₂ Henry's law constant by a factor of two in the model. Note that a large peak in the mid-troposphere at Hawaii in the models results from volcanic SO₂ emission.

5.2 Aerosol mass budgets and distributions

Globally and annually averaged budgets of aerosols in the TOMAS model are shown in Table 5 and are compared with the multi-model mean presented in Textor et al. (2006) – hereafter, referred to as AEROCOM mean. Additionally, we use the ACCMIP multi-model mean from Shindell et al. (2013) and Lee et al. (2013a), which is based on 8 ACCMIP models using the same AR5 emission scenario, to compare the sulphate and BC budgets. Note that the biomass burning emission in this study is GFEDv3 inventory averaged from 1997 to 2009, while the ACCMIP models use GFEDv2 inventory for 2000. We do not compare our model budget to the newer AEROCOM model burden mean presented in Myhre et al. (2013a) because most of their burden information is

not comparable to TOMAS; TOMAS does not separate the burden of carbonaceous aerosols by source category, which is the case in Myhre et al. (2013).

For sulphate, the total source rate (43.7 Tg yr^{-1}) is lower than the AEROCOM mean ($59.67 \text{ Tg S yr}^{-1}$), and the global burden (0.67 Tg S) is almost the same as the AE-
5 ROCOM mean burden (0.66 Tg S) due to the slightly longer lifetime in the TOMAS model (5.6 days vs. 4.1 days). As shown from the deposition coefficients (the inverse of the lifetime), the dry deposition coefficient is particularly small in TOMAS. Wet deposition accounts for 98 % of the total deposition, which is much higher than the AE-
10 ROCOM models, and moist convective clouds contribute 27 % of the wet deposition.
Similar to the AEROCOM mean comparison, the TOMAS total source rate is lower
than the ACCMIP mean (43.7 Tg yr^{-1} vs. $51.7 \text{ Tg S yr}^{-1}$), and the global burden is the
same as the ACCMIP mean burden (0.67 Tg S) due to the slightly longer lifetime in
the TOMAS model (5.7 days vs. 5.0 days). Note that GISS-E2-R-TOMAS included in
Shindell et al. (2013) is a basically identical model to the ModelE2-TOMAS, but the
15 sulphate budget in the two TOMAS models is different because the sulphate and DMS
emissions assumptions used in GISS-E2-R-TOMAS are similar to those used in the
bulk aerosol model in this paper.

Global-annual EC and OM burdens in TOMAS are 0.19 Tg and 1.2 Tg , respectively, which are roughly 70–80 % of the AEROCOM mean values (0.24 Tg for EC and
20 1.7 Tg for OM). The EC burden is similar to the ACCMIP multi-model mean from Lee et al. (2013a). The lower EC/OM burdens can be due to the lower emissions used in this model (7.4 Tg vs. 11.9 Tg for EC and 60.8 Tg vs. 96.6 Tg for OM). For EC and OM, their lifetimes are longer than the AEROCOM means but still within the standard deviation. Similar to sulphate, wet deposition contributes > 95 % of total deposition, which
25 is much higher than the AEROCOM mean, and 24 % of wet deposition is by moist convective clouds. Despite smaller dry deposition coefficients for EC and OM compared to the AEROCOM mean, their wet deposition coefficients are quite comparable to the AEROCOM mean.

[Title Page](#)[Abstract](#)[Introduction](#)[Conclusions](#)[References](#)[Tables](#)[Figures](#)[◀](#)[▶](#)[◀](#)[▶](#)[Back](#)[Close](#)[Full Screen / Esc](#)[Printer-friendly Version](#)[Interactive Discussion](#)

The global annual burden of sea salt and dust in TOMAS are 3.6 Tg and 9.1 Tg, respectively, which are about half of the AEROCOM mean values. Since their overall lifetime values are similar to the AEROCOM mean (0.4 days for sea salt and 4.7 days for dust), the lower burden can be explained by the lower emissions. For sea salt and

- 5 dust, dry deposition is as important as wet deposition due to their large particle sizes, accounting for 68 and 52 % of total deposition, respectively. Unlike the other aerosol species, the total removal rate coefficients for sea salt and dust are much lower than the AEROCOM mean values (5.1 day^{-1} for sea salt and 0.31 day^{-1} for dust) but very close to the AEROCOM median values (2.5 day^{-1} for sea salt and 0.25 day^{-1} for dust).
10 Looking at Fig. 5 of Textor et al. (2006), there is an outlier model (or more than one model) in the AEROCOM study, which has a significantly faster removal rate and increases the mean value. In the case of lifetime, the AEROCOM mean and median values are similar: their mean is more affected by a model with slower removal rate (longer lifetime).

15 Despite the same host model and the same anthropogenic emission scenarios as the TOMAS model, the bulk aerosol model shows significantly different aerosol mass budgets (in Table 6), which must arise from using different deposition assumptions and other aerosol modelling treatments (see Sect. 2 for the details). Sulphate burden and lifetime in the bulk aerosol model is roughly half of that in the TOMAS model.

- 20 The total source rate of SO_4 is about 20 % higher than TOMAS and is close to the AEROCOM mean value. The bulk aerosol model has a shorter lifetime for EC, leading to ~ 40 % lower burden compared to TOMAS. The OM burden is quite similar between two models. SOA formation rate is slightly different (14.6 Tg yr^{-1} for the bulk aerosol model and 17.1 Tg yr^{-1} for TOMAS), but the difference is only a small portion (about 25 3–4 %) of the total OM source rate. The sea-salt emission rate is lower than that in TOMAS due to the maximum size cutoff of $8 \mu\text{m}$ assumed in sea-salt emission, but its burden is more than a factor of two higher. For dust particles, the emission rate is higher than that in TOMAS due to the coarser size cutoff in their emissions (i.e. up to $16 \mu\text{m}$), and the burden is higher. For sea salt, the contribution of wet deposition to total

**ModelE2-TOMAS:
global aerosol
microphysics model**

Y. H. Lee et al.

[Title Page](#)[Abstract](#)[Introduction](#)[Conclusions](#)[References](#)[Tables](#)[Figures](#)[◀](#)[▶](#)[◀](#)[▶](#)[Back](#)[Close](#)[Full Screen / Esc](#)[Printer-friendly Version](#)[Interactive Discussion](#)

deposition is more than 2 times higher than that in TOMAS as well as the AEROCOM mean. Unlike the TOMAS model, the bulk aerosol model has nitrate aerosol, which has a global burden of 1.6 Tg with a lifetime of 6.4 days.

The removal rate coefficient of dry deposition is about 50–60 times higher for sulphate, EC and OM and about a factor of two higher for dust in the bulk aerosol model, making it more comparable to the AEROCOM mean values. The lower dry deposition rates with the TOMAS model is likely due to the size-dependent dry deposition parameterization. The dry deposition velocity is not saved in the ModelE2 output currently, so alternatively we refer to the Fig. 1 in Adams and Seinfeld (2001) that presents the global and annual-average of size-resolved dry deposition velocities in GISS-TOMAS (sulphate alone) compared to the size-independent one. Although the dry deposition velocities from ModelE2-TOMAS might not be exactly the same as the ones in the model version used in Adams and Seinfeld (2001) due to the updates made in ModelE2 (e.g. the boundary layer module), this point should be valid because the dry deposition parameterizations in the bulk and TOMAS models have been little changed. Despite the large differences in dry deposition rates for accumulation mode particles, dry deposition is a fairly minor removal pathway in both TOMAS and the bulk aerosol model.

Figure 6 shows simulated global distributions of annual-mean concentrations of TOMAS sulphate, EC, OM, sea salt and dust in the lowermost layer. The sulphate concentrations are high over industrial regions, driven by the SO_2 emissions and $\text{OH}/\text{H}_2\text{O}_2$ oxidant concentrations. Simulated EC and OM concentrations are high over the biomass burning regions and the industrial regions, especially East Asia and South Asia, but the OM concentrations are particularly pronounced over biomass burning regions due to their higher emissions. The sea salt concentrations are distributed fairly uniformly over the oceans but are higher over the Southern Ocean and lower over the oceans near the tropics as expected due to wind speed variations. The dust concentrations are pronounced over the source regions such as Northern Africa, Arabia, Northern/Northwestern China, and Australia.

[Title Page](#)[Abstract](#)[Introduction](#)[Conclusions](#)[References](#)[Tables](#)[Figures](#)[◀](#)[▶](#)[◀](#)[▶](#)[Back](#)[Close](#)[Full Screen / Esc](#)[Printer-friendly Version](#)[Interactive Discussion](#)

Figure 7 shows zonal distributions of annual-mean aerosol concentrations in TOMAS. The sulphate concentrations are highest between 0 and 50° N due to the high anthropogenic emissions in the NH. Over the SH, the sulphate concentrations are mostly a result of DMS oxidation. The zonal-mean EC and OM concentrations are high from the tropics to ~ 50° N. Similar to Fig. 6, the high EC and OM concentrations are around 30 to 50° N due to fossil fuel emissions, but the OM concentrations are also large around the tropics due to biomass burning emissions. The sea salt concentrations are high from 60° S to 50° N with a peak around 30 to 60° S due to the large open ocean in the SH. For the dust concentrations, a strong peak is shown at around 0–30° N due to the strong Northern African emissions, and a weak peak at around 30° S due to Australian emissions.

5.3 Aerosol mass concentrations evaluation

The simulated surface-layer mass concentrations of aerosols are evaluated against various observations: (1) sulphate/sea salt/dust concentrations at 23 long-term observation sites operated by University of Miami (e.g. Prospero and Bonatti, 1969; Savoie and Prospero, 1989; Arimoto et al., 1990), (2) speciated PM_{2.5} concentrations from the Interagency Monitoring of Protected Visual Environment (IMPROVE) sites in the United States that are annual-averages from 2000 to 2008 (Debell et al., 2006; Hand et al., 2011), (3) speciated PM_{2.5} concentrations from various European observations (Putaud et al., 2010) (hereafter, referred to as European sites), (4) a large set of PM_{2.5} observations assembled in support of the Global Burden of Disease Study (GBD Study 2010, <http://www.globalburden.org>), (5) deposition flux measurements obtained from Ginoux et al. (2001), Tegen et al. (2002), and Mahowald et al. (2009). The PM_{2.5} dataset from the GBD Study consists of a worldwide set of annual-average PM_{2.5} largely drawn from official monitoring networks for 2005 (in some cases from 2004–2006). The GBD PM_{2.5} dataset includes the IMPROVE network and the European site measurements, so we only present the PM_{2.5} evaluation with the GBD dataset. The

[Title Page](#)[Abstract](#)[Introduction](#)[Conclusions](#)[References](#)[Tables](#)[Figures](#)[◀](#)[▶](#)[◀](#)[▶](#)[Back](#)[Close](#)[Full Screen / Esc](#)[Printer-friendly Version](#)[Interactive Discussion](#)

details of the GBD PM_{2.5} dataset are referred to the description in the supplementary material in Shindell et al. (2011).

Figure 8 compares the model annual-mean surface-layer sulphate mass concentrations to the observations from the IMPROVE network, the European sites, and the University of Miami network. Simulated sulphate agrees well with observations, mostly within a factor of two. Compared to the bulk aerosol model, the TOMAS model shows better agreement in the European sites (i.e. LMNB = -0.06 and LMNE = 0.13) but worse in the IMPROVE sites (i.e. LMNB = 0.06 and LMNE = 0.16) and the remote oceanic sites (i.e. LMNB = 0.04 and LMNE = 0.22). Over the US, both models over-predict systematically at lower observed concentrations (i.e. below 1 µg m⁻³ of measured SO₄ concentrations), which are mostly located over the western US. For TOMAS, a large overprediction is also observed at a few remote marine sites that are mostly located in SH marine regions where DMS oxidation is the main source for SO₂ and thus SO₄.

Monthly mean surface-layer sulphate concentrations are evaluated using observations from the University of Miami in Fig. 9. The simulated sulphate mass concentrations from both models usually falls within the standard deviation of the observed values. The sulphate predictions in both the bulk aerosol model and TOMAS become quite similar over the SH because about a factor of two lower DMS emissions are used in TOMAS. Using the same DMS emissions as the bulk aerosol model, TOMAS tends to overpredict sulphate concentrations noticeably over the SH (not shown), and the higher SO₄ concentration with TOMAS could be explained by (1) a longer lifetime due to different deposition parameterizations, (2) letting all SO₄ formed from aqueous oxidation to evaporate without accounting for cloud evaporation, (3) a stronger oxidation state resulted from un-degraded photolysis rates by aerosol optical depth (more SO₄ can be formed from DMS oxidation). Despite the fact that the bulk aerosol model accounts for the heterogeneous SO₄ formation on dust particles, SO₄ concentrations in near dust source regions are still higher in the TOMAS model due to the shorter lifetime in the bulk aerosol model.

[Title Page](#)[Abstract](#)[Introduction](#)[Conclusions](#)[References](#)[Tables](#)[Figures](#)[◀](#)[▶](#)[◀](#)[▶](#)[Back](#)[Close](#)[Full Screen / Esc](#)[Printer-friendly Version](#)[Interactive Discussion](#)

Simulated annual-mean surface-layer sea salt concentrations are evaluated with the IMPROVE network, the European sites, and the University of Miami network (Fig. 10). Both aerosol models are biased strongly high over the US and Europe but biased low near the tropics. Unlike the bulk aerosol model, TOMAS underpredicts sea salt

5 concentrations at several remote sites. Compared to other aerosol components, the agreement between model sea salt and the observations is worse over the United States and Europe. For the evaluation of monthly mean surface-layer sea salt concentrations against the University of Miami dataset in Fig. 11, the model predictions fall within the observed standard deviation at about a half of the 26 sites, but these sites
10 are not necessarily the same between the two aerosol models. Both models tend to be biased significantly low at some of the sites near the tropics. The bulk aerosol model exhibits a particularly large overprediction over most SH sites.

For TOMAS, simulated annual-mean surface-layer dust concentrations are mostly within a factor of two of the measurements (in Fig. 12): 6 sites are excluded in Fig. 12
15 due to an incomplete annual cycle. TOMAS shows good agreement at the IMPROVE and European sites, while the bulk aerosol model tends to underpredict. Both models are biased low compared to the University of Miami dataset, and only 7–8 sites among 20 sites fall within a factor of two agreement. A few sites show a severe underprediction, mostly located near the tropics and in SH high latitudes.

20 Monthly mean surface-layer dust concentrations are evaluated using the observations from the University of Miami in Fig. 13: no measurement data is available at 3 sites (Reunion Island, Invercargill, and Marion Island), but we still include them to compare the two aerosol model predictions. The model captures the observed annual cycle of dust very well at most NH sites but not in the SH sites except Norfolk and Mawson.

25 The model captures the observed magnitude well at sites located relatively near the source regions (e.g., Sal Island, Barbardos, Bermuda for African dust; Jeju Island and Hedo for Asian dust; Cape Grim and Norfolk Island for Australian dust). Both models underpredict dust concentrations in the NH/SW high latitude (45°) regions except Mace Head, but the simulated dust seems to be within the observed standard deviation as

Title Page	
Abstract	Introduction
Conclusions	References
Tables	Figures
◀	▶
◀	▶
Back	Close
Full Screen / Esc	
Printer-friendly Version	
Interactive Discussion	



the observations have a large standard deviation for dust. Interestingly, the observed peak concentration at Heimaey Iceland is the second highest after Sal island, and the models underpredict this severely, which is also shown in GISS-TOMAS (Lee et al., 2009).

Figure 14 compares simulated annual-mean dust deposition fluxes against observations obtained from Ginoux et al. (2001), Tegen et al. (2002), and Mahowald et al. (2009). Data is classified by the influencing source region, presented in different colours in Fig. 14. Except for the minor source category, the model dust deposition fluxes tend to be underestimated at most locations and agree with observations only within a factor of 5–8 on average. This may indicate that dust emissions are too low in ModelE2, but deposition fluxes measurements could contain large particles especially close to source regions (e.g., Duce, 1995) or local emissions (Uematsu et al., 1985) that are not simulated in the model. For TOMAS, the upper size limit being 10 µm, which is too small for the dust particles near the sources, can explain some of the severe underprediction, and Lee et al. (2009) also shows similar disagreement using the GISS-TOMAS model.

Figure 15 shows simulated annual-mean surface-layer BC and OM concentrations compared against the observations from the IMPROVE network and the European sites from Putaud et al. (2010). The simulated BC and OM are within a factor of 2 on average at the IMPROVE sites and within a factor of 2–3 at the European sites. The model OM is slightly underpredicted at the IMPROVE sites (LMNB is –0.19 for TOMAS and –0.28 for the bulk aerosol model), and this is partly due to OM/OC ratio of 1.4 used in the model: the OM from the IMPROVE network uses OM/OC ratio of 1.8, but the ratio is 1.4 for the European sites. When using a consistent conversion from OC to OM between the models and the IMPROVE observation, LMNB is improved from –0.19 to –0.08 for TOMAS and from –0.28 to –0.17 for the bulk aerosol model (not shown).

Figure 16 compares simulated annual-mean PM_{2.5} concentrations against the GBD dataset. Note that the bulk aerosol model includes nitrate mass into its PM_{2.5}, and the nitrate contributes to PM_{2.5} rather significantly. The GBD data is classified/presented

Title Page	
Abstract	Introduction
Conclusions	References
Tables	Figures
◀	▶
◀	▶
Back	Close
Full Screen / Esc	
Printer-friendly Version	
Interactive Discussion	



by a region listed in Fig. 16a and b. The aerosol models capture the observation quite well in most locations (overall LMNB is -0.08 and LMNE is $0.2\text{--}0.24$), but both models show the worst agreement for Oceania regions ($\text{LMNB/LMNE} = 0.4\text{--}0.47$) and Latin America ($\text{LMNB/LMNE} = -0.33$ to -0.53). The overpredicted $\text{PM}_{2.5}$ in Oceania might be consistent with the sulphate evaluation with the Miami dataset shown in Fig. 9. Figures 11 and 13 show severely underpredicted sea salt or dust particles in several sites in Oceania, but they are mostly coarse particles. The underprediction of $\text{PM}_{2.5}$ in Latin America might be related to the biomass burning emissions. It is consistent with the model AOD being biased low over biomass burning source regions that is shown in Sect. 5.4. Model evaluation with the observed PM_{10} concentrations using the IMPROVE and European sites was also performed and is similar to the $\text{PM}_{2.5}$ evaluation results (not shown): LMNB and LMNE are -0.01 and 0.17 for TOMAS and 0.0 and 0.29 for the bulk aerosol model, respectively.

5.4 Aerosol optical depth evaluation

Simulated annual-mean clear-sky aerosol optical depths (AODs) at 550 nm are compared with observations from the Terra MODIS (MODerate resolution Image Spectroradiometer; e.g. Abdou et al., 2005; Remer et al., 2008) and MISR (Multiangle Image SpectroRadiometer; e.g. Diner et al., 1998; Kahn et al., 2005) satellite instruments averaged over 2004–2006 (Fig. 17). We use the Deep Blue AOD (e.g., Hsu et al., 2006) from Terra MODIS to increase its spatial coverage, and all the satellite data was obtained from <http://disc.sci.gsfc.nasa.gov/giovanni>. When the Deep Blue AOD and the “regular” AOD from Terra MODIS are both available, the former is used. However, we notice that the Deep Blue AOD shows some local hotspots (e.g. over South America) that are not shown in the “regular” MODIS AOD as well as the MISR AOD. Our model calculates clear-sky AOD by including only AOD values calculated in model locations where clouds are not present. The TOMAS and bulk aerosol models capture the broad spatial features seen in the satellite measurements: (1) very high AODs over desert regions in and near Northern Africa and the Arabian Peninsula associated with mineral

dust, (2) the band of locally enhanced AOD over the Southern Ocean associated with sea salt, (3) high AODs over East Asia and India due to high anthropogenic emissions. However, the models underestimate the AOD over East Asia and the Indo-Gangetic plain, especially compared to MODIS. Including nitrate in the bulk aerosol model, the 5 AOD predictions increase particularly over Europe and East Asia. Without nitrate, they become quite similar to the TOMAS AOD values in the regions where the model nitrate predictions are significant. The models show an enhanced AOD over the biomass burning regions such as tropical South America, Africa and Indonesia but it is clearly underestimated. The simulated AOD in North America and high latitude regions appears 10 also to be lower than the satellite observations. Comparing with the bulk aerosol model AOD, TOMAS shows a stronger AOD over Africa due to its higher dust burden and a lower AOD over the marine areas especially the Southern Ocean associated with sea salt.

We present spatial correlations and biases between the models and the satellite 15 data (Table 7). For these analyses, the annual-mean satellite AOD fields are regridded to $2^\circ \times 2.5^\circ$ horizontal resolution, and the models are sampled only where the satellite AOD is available. Correlation coefficients between the model and satellite AODs are around 0.6–0.7 for TOMAS and around 0.4–0.5 for the bulk aerosol model. Given that the correlation coefficient between MODIS and MISR is 0.79, the TOMAS model shows 20 a good correlation with these satellite data. Both models show better correlations with MISR AOD. Compared to the bulk aerosol model, TOMAS shows a strong negative bias (about –29 to –34 %) for both satellite datasets because of noticeably low AODs over the oceanic regions (where sea salt is dominant) shown in Fig. 16 and possibly because of missing component such as nitrate aerosols, which contributes to AOD significantly 25 over Europe and China in the bulk aerosol model. Over Europe, the bulk aerosol model overpredicts AOD due to nitrate though. Without nitrate in the bulk aerosol model, the normalized mean bias (NMB) falls from 8–16 % to –16 to –21 %. Both models show lower AOD over China, India, and biomass burning regions, indicating a possibility of aerosol emissions being underestimated in these regions.

[Title Page](#)
[Abstract](#) [Introduction](#)
[Conclusions](#) [References](#)
[Tables](#) [Figures](#)
[◀](#) [▶](#)
[◀](#) [▶](#)
[Back](#) [Close](#)
[Full Screen / Esc](#)
[Printer-friendly Version](#)
[Interactive Discussion](#)



Figure 18 presents simulated monthly mean AODs compared against AERONET (AErosol RObotic NETwork; Holben et al., 1998, 2001) measurements at 28 sites that represent the following characteristic regions: polluted continental, marine, biomass-burning, and dusty regions (see Table 8 for individual site information). Both the TOMAS and the bulk aerosol models underestimate the maximum AOD during summer by a factor of 2–3 in the biomass burning sites (1 to 6) but capture the observed annual cycle quite well ($R \geq 0.9$). Unlike other biomass burning sites, simulated AODs at Ilorin and Banizoumbou are comparable to the observations possibly due to the influence of mineral dust. The agreement between the models and the AERONET AOD is generally good in the dusty regions (9 to 16). The TOMAS model shows a slight overprediction of AOD during spring at Capo Verde and Bidi Bahn which are located near the African dust sources, although it shows a good agreement at Barbados where is also influenced by African dust.

For TOMAS, all polluted continental sites (17 to 24) show large underpredictions, while the model tends to capture the observed annual cycle well. However, the model surface aerosol mass concentrations agree well with the observations from IMPROVE network and several European sites (see Figs. 8, 10, 12, 15, and 16). This might be due to the fact that column AOD depends on many additional factors (e.g., optical properties and vertical distribution of aerosols) and provides a measure of total radiatively active aerosols in the atmosphere. Misrepresentation of these factors or missing a chemical component could introduce a bias in the model AODs. For the bulk aerosol model, the model AOD without nitrate is quite similar to the TOMAS AOD. Including nitrate in the bulk aerosol model, it simulates the annual-mean AERONET AOD relatively well but the observed annual cycle worse. Although the inclusion of nitrate is helpful for the underpredicted AOD in polluted regions, the overprediction of wintertime AOD suggests that the model nitrate is too large.

With the TOMAS model, the oceanic sites (25 to 30) are generally underpredicted roughly by a factor of two except for Bermuda (25) and Lanai (26). In contrary, the bulk aerosol model captures the observed magnitude relatively well but overpredicts at

[Title Page](#)[Abstract](#)[Introduction](#)[Conclusions](#)[References](#)[Tables](#)[Figures](#)[◀](#)[▶](#)[◀](#)[▶](#)[Back](#)[Close](#)[Full Screen / Esc](#)[Printer-friendly Version](#)[Interactive Discussion](#)

Bermuda and Lanai. Note that Bermuda (23) and Rottnest Island (27) are influenced by long-range transported mineral dust. The bulk aerosol model predicts AOD that is more comparable to observations in these oceanic sites than TOMAS. Compared to the bulk aerosol model, the underprediction of sea salt concentrations at the remote sites (shown in Figs. 10 and 11 in Sect. 5.3) and the underpredictions of AODs in the remote oceanic sites in ModelE2-TOMAS may be due to a faster sea salt removal rate (see global budgets in Table 5 for the details). It is worth mentioning that the inclusion of marine organic aerosols, which are not included in this paper, may not increase AOD noticeably in remote oceanic sites. Using the same host model, Tsigaridis et al. (2013) shows that Southern Ocean AOD is quite insensitive to the inclusion of marine organic particles but is strongly sensitive to the sea-salt emissions parameterization (see Fig. 9 of Tsigaridis et al., 2013).

5.5 Aerosol number budgets and its distributions

This section includes only TOMAS results, as the bulk aerosol model does not predict aerosol number concentrations. Global mean number budgets for all three simulations, including two sensitivity runs for nucleation rates, are presented in Table 9 (see Sect. 4.2 and Table 1 for the details of run descriptions). Compared to the BASE run, global mean CN3 (particles with diameters larger than 3 nm), CN10 (particles with diameters larger than 10 nm), and CN100 (particles with diameters larger than 100 nm) concentrations in the LowNUC run are decreased by 74, 33, and 7 % in the troposphere and 29, 17, and 3 % in the lowermost layer, respectively. The smaller impact on CN in the lowermost layer is obviously due to the presence of the primary emissions near the surface. It is also because the binary nucleation parameterization used in this model produces few particles in the boundary layer; however, nucleated particles in the upper/free troposphere may be carried down to the surface and influence CN there. Since the LowNUC run produces fewer nucleated particles than the BASE run, each nucleated particle is more likely to grow more efficiently to form CCN-sized particles, as there is less competition for sulphuric acid and condensable organics.

Title Page	
Abstract	Introduction
Conclusions	References
Tables	Figures
◀	▶
◀	▶
Back	Close
Full Screen / Esc	
Printer-friendly Version	
Interactive Discussion	



Aerosol number burdens are dramatically reduced when nucleation is turned off in the NoNUC run. For example, global mean CN3 and CN10 are decreased by 95 and 76 % in the troposphere and by 42 and 31 % in the surface layer. We found that 24 % of tropospheric CCN-sized particles (i.e., CN100) and ~ 10 % of surface-layer CCN-sized particles result from binary nucleation in our model; the contribution of the nucleated particles to the CCN concentrations is larger as the cutoff size (e.g. 100 nm in CN100) gets lower.

Figure 19 shows global distributions of annually averaged CN3, CN10, and CN100 in the lowermost layer for the BASE, LowNUC, and NoNUC runs, and Fig. 20 presents their zonal distributions. For the CN3 distributions, the BASE run shows a high concentration (over 5000 cm^{-3}) in the upper/free troposphere and the entire Antarctica troposphere due to nucleation and over polluted continental regions due to the primary emissions. Note that the CN3 near the surface in Antarctica comes from nucleated particles from the upper/free troposphere, as the binary parameterization does not predict nucleation in the boundary layer. CN3 in the LowNUC run is decreased significantly in the free troposphere and in the surface layer over Eurasia and western Antarctica (fewer nucleated particles formed above subside to the surface). Obviously, when turning nucleation off, CN3 is very close to CN10, and has only a single maximum concentration near the surface in the NH, due to anthropogenic emissions. For CN10, its spatial pattern over the continents is quite similar among the runs as it is mostly driven by primary emissions except for some locations heavily influenced by the nucleated particles formed in the upper/free troposphere. A pronounced difference in CN10 is shown over oceans, indicating a larger contribution of nucleated particles to CN10 in these regions. This is consistent with Merikanto et al. (2009), which shows higher contribution of nucleation to CN over oceanic regions. CN100 differs little among runs except for SH high latitudes where binary nucleation plays an important role, which is consistent with Pierce and Adams (2009) showing that the exhibited high SH latitude region for the most positive changes in CCN (0.2 %) by turning on binary nucleation and, again, with Merikanto et al. (2009) showing 65 % of CCN (0.2 %) in Antarctica

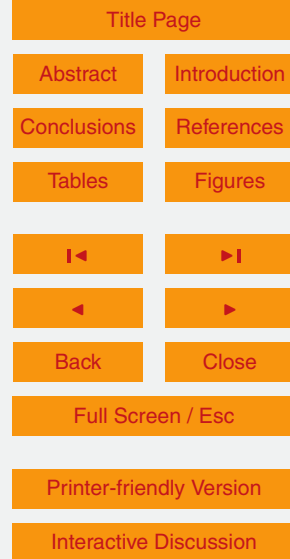
[Title Page](#)[Abstract](#)[Introduction](#)[Conclusions](#)[References](#)[Tables](#)[Figures](#)[◀](#)[▶](#)[◀](#)[▶](#)[Back](#)[Close](#)[Full Screen / Esc](#)[Printer-friendly Version](#)[Interactive Discussion](#)

resulted from upper tropospheric nucleation. CN100 shows a maximum at 10 to 40° N because most anthropogenic emissions are located in mid-NH latitudes. Rather surprisingly, dust particles in our model contribute to CN100 quite significantly over the source regions.

5 5.6 Aerosol number evaluation

The CN measurement dataset compiled by Spracklen et al. (2010) is used to evaluate simulated annual-mean CN concentrations (in Fig. 21) and monthly mean CN concentrations (in Fig. 22). Details of the measurement procedures for each site, including the instrument type and minimum cutoff diameter (varying from 3 to 14 nm), can be found in Table 2 of Spracklen et al. (2010). Due to an incomplete annual cycle, we excluded Mt. Waliguan, Finokalia, Listvyanka, and Weybourne. The measurement sites are classified into three categories: FT (free troposphere; 8 sites from Zugspitze to South Pole in Fig. 22), MBL (marine boundary layer; 7 sites from Point Barrow to Neumayer in Fig. 22), and CBL (continental boundary layer; 17 sites from Pallas to Botsalano in Fig. 22). We sampled the model values to match the altitude of each measurement site except for the free troposphere sites that use an altitude 30 % lower because it improved the annual cycles prediction significantly. Previous studies pointed out that free tropospheric sites can be influenced by upslope winds that carry the planetary boundary layer air, so it cannot be assumed to be in the free troposphere all the time (e.g., Baltensperger, 1997; Collaud Coen et al., 2011). Our model does not seem to simulate this well, so sampling the model predictions at lower altitude (i.e., 30 % lower) helps to increase the influence of PBL air. In Fig. 21, a whisker plot is used to present the three run results; the maximum of the whisker line for the BASE run; the circle symbol in the middle of the whisker line for the LowNUC run; the minimum for the NoNUC run.

25 On average, the annual-mean CN concentrations in the model agree with the observations well for the all three categories ($LMNB = -0.26\text{--}0.16$; $LMNE = 0.13\text{--}0.22$). Simulated annual cycles at individual sites also show that the model captures the measured magnitude reasonably but overpredicts the CN during winter (November to March) that



Title Page	
Abstract	Introduction
Conclusions	References
Tables	Figures
◀	▶
◀	▶
Back	Close
Full Screen / Esc	
Printer-friendly Version	
Interactive Discussion	



is worse at the CBL sites and results in poor seasonality (especially in the BASE run). The poor seasonality in ModelE2-TOMAS in all three runs suggests that other factors may play a role such as missing seasonal variation in primary emissions or scavenging that causes the poor seasonality rather than nucleation. The evaluation of CN at South Pole shows that the model predicts too strong nucleation throughout the year.

Figure 23 compares the observed size distributions at six European sites during winter (DJF: December to February) and summer (JJA: June to August) to the model. Note that the observed size distributions are averaged during morning, afternoon, and night, while the model results are not broken into the three periods. As expected, the simulated size distributions of the model simulations differ according to what nucleation scheme is used. The impact of nucleation is more notable for particles smaller than ~50 nm, as expected, and also during winter. In general, the higher nucleation rates tend to overpredict Aitken model particles at most sites. For Harwell, particles below 50 nm are overpredicted even without nucleation. For the summer season, the model shows less sensitivity to nucleation rates and has better skill at capturing the observed size distributions.

The observed CN5, CN15, and CN120 concentrations from the LACE campaign (Petzold et al., 2002) are compared with three model runs (Fig. 24a). Below 700–800 mbar, all three model runs predict concentrations roughly within the observed CN5, CN15, and CN120 ranges. Above 700–800 mbar, the BASE simulation overpredicts CN5 and CN15 by approximately an order of magnitude and 2–3 times, respectively. For the NoNUC simulation, it captures the lower side of the observed CN15 but fails to capture the increasing CN5 concentrations with height above 600 mbar. All model runs basically show almost identical CN120 concentrations and fall on the lower edge of the observed range.

Figure 24 compares CN3 vertical profile measurements averaged into the 3 latitude bands over the Pacific Ocean (Clarke and Kapustin, 2002) with the model. The simulated CN3 profiles in LowNUC agree well with the observation, capturing the increasing CN3 with height. Although the BASE run shows the increasing pattern correctly, it

overpredicts CN3 severely above approximately 6 km. The NoNUC run disagrees with the observations for all latitudes and altitudes and clearly fails to reproduce the high number concentrations in the upper troposphere that result from nucleation.

The observed Aitken mode and accumulation mode concentrations and size distributions in the marine boundary layer (Heintzenberg et al., 2000) are compared with the model in Figs. 25 and 26. The measurements are aggregated into 15° latitude ranges. For the accumulation mode, the three model runs are quite similar to each other and are within the observed range. For the Aitken mode, the LowNUC run shows the closest agreement to observations. However, whereas the observations show higher concentrations in the SH than in the NH, all model simulations show the opposite tendency. Similarly, other global models with binary nucleation show underpredicted CN concentrations in the SH and either well-simulated or overpredicted CN in the NH (e.g. Easter et al., 2004; Spracklen et al., 2005; Pierce and Adams, 2006; Pierce et al., 2007; Trivitayanurak et al., 2008; Mann et al., 2010; Wang et al., 2011).

In Fig. 26, ModelE2-TOMAS captures the bimodal size distribution shown in the observations reasonably, which is mainly determined by the activation diameter assumed in wet deposition (and cloud processing): ~ 80 nm as an activation diameter (supersaturation of 0.2 %) for both large-scale clouds and convective clouds in the model. Note that ModelE2-TOMAS cannot capture the observed bimodal distribution when a supersaturation of 1.0 % is assumed for convective clouds, unlike the other TOMAS models (e.g. Pierce et al., 2007; Trivitayanurak et al., 2008): a peak at around 20–30 nm appears when the supersaturation of 1.0 % is assumed for convective clouds. This suggests that, compared to GISS GCM II', moist convective clouds are more frequent in ModelE2. Although the model captures the observations successfully using fixed supersaturation assumptions, future work is needed to link the in-cloud supersaturation to cloud and aerosol properties.

Simulated CCN concentrations are compared against a dataset of CCN measurements compiled by Spracklen et al. (2011) in Figs. 27 and 28: see Table 1 in Spracklen et al. (2011) for the details regarding each site. The CCN dataset includes a total of 277

[Title Page](#)[Abstract](#)[Introduction](#)[Conclusions](#)[References](#)[Tables](#)[Figures](#)[◀](#)[▶](#)[◀](#)[▶](#)[Back](#)[Close](#)[Full Screen / Esc](#)[Printer-friendly Version](#)[Interactive Discussion](#)

measurements at 80 locations using various instruments from 1971 to 2009. Approximately 70 % of the observations were taken after 1990. Most have sampling periods of days to weeks except the observations at Cape Grim and Mace Head. For Cape Grim and Mace Head, an annual cycle is available, so we present them separately in Fig. 28. In Fig. 27, the CCN data is divided into two groups: CCN in the MBL (marine boundary layer) and the rest (referred as to “CCN not in MBL”). For “CCN not in MBL”, the model CCN shows good agreement with the observation in all three simulations ($LMNB = 0.11\text{--}0.2$ and $LMNE = 0.31\text{--}0.34$). For CCN in the MBL, the model predictions are, on average, within a factor of 1.5–2 of the observations for all three runs but, relative to several measurements of CCN concentration between ~ 100 and $\sim 300 \text{ cm}^{-3}$, are biased high, by roughly a factor of two. For the annual cycle of CCN concentrations at Cape Grim and Mace Head (Fig. 28), the model overpredicts in all months even without nucleation ($NMB > 1.0$). The CCN overpredictions at Cape Grim might be influenced by overpredicted SO_2 (shown in Fig. 3), which could lead to overpredicted condensational growth of Aitken mode particles. As with the SO_2 evaluation in Fig. 3, the CCN overprediction decreases by sampling adjacent grids toward the ocean (not shown), but the model CCN is still higher than the measurements. Given the fact that most CCN observations have very short duration (days to weeks) in a single year and, according to Spracklen et al. (2011), the relative uncertainties in the measurement data range from about 5–40 %, mostly in 10–20 % very roughly, the overall model-to-observation agreement is satisfying.

6 Conclusions

We have implemented the TwO-Moment Aerosol Sectional (TOMAS) microphysics model into the new version of the GISS GCM (i.e. ModelE2), called “ModelE2-TOMAS”. This paper has compared the global budgets of ModelE2-TOMAS to other global aerosol models and evaluates the model with various observations such as aerosol

Title Page	
Abstract	Introduction
Conclusions	References
Tables	Figures
◀	▶
◀	▶
Back	Close
Full Screen / Esc	
Printer-friendly Version	
Interactive Discussion	



precursor gas concentrations, aerosol mass and number concentrations, and aerosol optical depth.

Global budgets of aerosols and aerosol precursor gases in ModelE2-TOMAS are similar to those in other global aerosol models, and the TOMAS model agrees reasonably (mostly within a factor of two) with long-term observed aerosol precursor gas and aerosol mass concentrations. The model captures the broad spatial features shown in the MODIS and MISR annual-mean AOD distributions as well as the observed seasonal trends of AOD at several AERONET sites. The model predicts the observed annual-mean CN (the minimum cutoff varying from 3 to 14 nm) concentrations very well and the observed vertical profiles of aerosol number over Germany (i.e., LACE campaign) and in the marine boundary layer. For CCN, the model shows good skill in capturing the observations. We conclude that the model is realistic enough to be useful for many types of scientific study.

However, the evaluations have also highlighted some weaknesses in ModelE2-TOMAS to be revisited in the future. First, ModelE2-TOMAS predicts too much SO₂ lifted into the upper/free troposphere over the Pacific Ocean possibly due to overly strong convective transport. This is also seen in the bulk aerosol model (and in gaseous tracers), suggesting this might be a host model problem. Second, the model AOD is underpredicted over polluted continents, even though mass concentrations of each aerosol component at the surface are well simulated (or at least not underpredicted) in the model. Missing nitrate in TOMAS may not be the main contributor, as the inclusion of nitrate in the bulk aerosol model decreases its ability to capture the observed seasonality in AERONET polluted continents sites. Third, the model tends to underpredict aerosol loading (and AOD) over biomass burning emission regions. This is a common issue in global aerosol models, and this might be due to underestimation of biomass burning emissions. Fourth, an TOMAS AOD prediction is biased low over the SH high-latitude oceans, which suggests underpredicted sea salt burden in this area. Fifth, the simulated CN seasonality is poor at some CBL sites due to overpredicted CN during the wintertime. Similarly, TOMAS predicts the observed number

[Title Page](#)[Abstract](#)[Introduction](#)[Conclusions](#)[References](#)[Tables](#)[Figures](#)[◀](#)[▶](#)[◀](#)[▶](#)[Back](#)[Close](#)[Full Screen / Esc](#)[Printer-friendly Version](#)[Interactive Discussion](#)

Title Page	
Abstract	Introduction
Conclusions	References
Tables	Figures
◀	▶
◀	▶
Back	Close
Full Screen / Esc	
Printer-friendly Version	
Interactive Discussion	

size distributions over European sites during the summer season reasonably but not for the winter season. The model overpredicts Aitken mode particles during the winter season, which happens even without nucleation, possibly due to a problem in primary emissions representation or a bias in the model scavenging that causes the poor seasonality. Finally, ModelE2-TOMAS seems to predict faster nucleation rates using binary nucleation (Vehkamaki et al., 2002) than other global microphysics models using the same binary nucleation (including GISS-TOMAS). For instance, the observed CN vertical profiles are captured the best when nucleation rates are reduced (our LowNUC run), while Lauer et al. (2005) presents significantly underpredicted CN profiles with the same binary nucleation scheme using ECHAM/MADE. To investigate this issue further, we need to perform a model evaluation against observation-derived nucleation-relevant metrics, which has been done in Westervelt et al. (2013). Because of the fine size assumptions for the primary emissions (see Sect. 4.2 for the details) and/or the fast nucleation rates using binary nucleation in ModelE2-TOMAS, we do not include boundary nucleation as it overpredicted CN near the surface. We conclude that further work is necessary to improve the realism of some aspects of ModelE2-TOMAS and to better understand the size-resolved physical processes (e.g. microphysics, emissions, and depositions).

Comparing the TOMAS model with the bulk aerosol model in ModelE2, some aerosol species burdens and concentrations differ significantly, even with using the same host model and identical anthropogenic emissions, mainly because the deposition parameterizations and some of the emission-related assumptions are different. In the case of sea salt and dust, the size ranges assumed by each model are different, resulting in different emission rates and burdens.

Analysis of multiple aerosol model results help to identify where a model bias might originate from: aerosol modelling or the host GCM or elsewhere such as emissions. We found that some of the large differences in aerosol predictions between the two aerosol models are due to aerosol modelling. This is valuable information, as this is not easy to constrain using observations. Having more than one aerosol physics representation in



ModelE2-TOMAS: global aerosol microphysics model

Y. H. Lee et al.

[Title Page](#)

[Abstract](#)

[Introduction](#)

[Conclusions](#)

[References](#)

[Tables](#)

[Figures](#)



[Back](#)

[Close](#)

[Full Screen / Esc](#)

[Printer-friendly Version](#)

[Interactive Discussion](#)



the NASA GISS ModelE2 will serve as a useful tool to study the uncertainty in aerosol modelling and to guide our efforts to improve the models.

Acknowledgements. Funding for this research was supported by NASA ACMAP and MAP program. Resources supporting the simulations were provided by the NASA High-End Computing (HEC) Program through the NASA Center for Climate Simulation (NCCS) at Goddard Space Flight Center. We gratefully acknowledge the mission scientists and Principal Investigators who provided the data used in this research effort (EMEP, CASTNET, IMPROVE, and University of Miami networks, AERONET, NASA MODIS and MISR). We also acknowledge the PIs for the CN and CCN surface measurements at the WMO-GAW sites (J. Ogren, Earth System Research Laboratory, NOAA, US; J. Gras, CSIRO Ocean and Atmosphere Flagship, Australia; U. Baltensperger, Paul Scherrer Institute, Switzerland; U. Kaminski, Deutscher Wetterdienst (DWD), Germany; S. G. Jennings, National University of Ireland Galway, Ireland; R. Weller, Alfred Wegener Institute for Polar and Marine Research, Germany; Y. Viisanen, Finnish Meteorological Institute, Finland). We further acknowledge that Cape Grim data are provided by the Australian Bureau of Meteorology (Cape Grim Baseline Air Pollution Station) and CSIRO Ocean and Atmosphere Flagship. We thank Graham Mann (University of Leeds, UK) and Dominick Spracklen (University of Leeds, UK) for providing aerosol number measurements data collection. We also thank Greg Faluvegi (NASA GISS) and Maxwell Kelley (NASA GISS) for providing technical support during the model development.

References

- Abdou, W. A., Diner, D. J., Martonchik, J. V., Bruegge, C. J., Kahn, R. A., Gaitley, B. J., Crean, K. A., Remer, L. A., and Holben, B.: Comparison of coincident Multiangle Imaging Spectroradiometer and Moderate Resolution Imaging Spectroradiometer aerosol optical depths over land and ocean scenes containing Aerosol Robotic Network sites, *J. Geophys. Res.-Atmos.*, 110, D10S07, doi:10.1029/2004jd004693, 2005.
- Adams, P. J. and Seinfeld, J. H.: Predicting global aerosol size distributions in general circulation models, *J. Geophys. Res.-Atmos.*, 107, 4370, doi:10.1029/2001JD001010, 2002.
- Arimoto, R., Ray, B. J., Duce, R. A., Hewitt, A. D., Boldi, R., and Hudson, A.: Concentrations, sources, and fluxes of trace-elements in the remote marine atmosphere of New-Zealand, *J. Geophys. Res.-Atmos.*, 95, 22389–22405, doi:10.1029/JD095iD13p22389, 1990.

[Title Page](#)

[Abstract](#)

[Introduction](#)

[Conclusions](#)

[References](#)

[Tables](#)

[Figures](#)



[Back](#)

[Close](#)

[Full Screen / Esc](#)

[Printer-friendly Version](#)

[Interactive Discussion](#)



Ayers, G. P., Ivey, J. P., and Gillett, R. W.: Coherence between seasonal cycles of dimethyl sulfide, methanesulfonate and sulfate in marine air, *Nature*, 349, 404–406, doi:10.1038/349404a0, 1991.

Baltensperger, U.: Aerosol climatology at the high Alpine site Jungfraujoch, Switzerland, *J. Geophys. Res.*, 102, 19707–19715, 1997.

Bauer, S. E. and Koch, D.: Impact of heterogeneous sulfate formation at mineral dust surfaces on aerosol loads and radiative forcing in the Goddard Institute for Space Studies general circulation model, *J. Geophys. Res.-Atmos.*, 110, D17202, doi:10.1029/2005jd005870, 2005.

Bauer, S. E., Koch, D., Unger, N., Metzger, S. M., Shindell, D. T., and Streets, D. G.: Nitrate aerosols today and in 2030: a global simulation including aerosols and tropospheric ozone, *Atmos. Chem. Phys.*, 7, 5043–5059, doi:10.5194/acp-7-5043-2007, 2007.

Bauer, S. E., Wright, D. L., Koch, D., Lewis, E. R., McGraw, R., Chang, L.-S., Schwartz, S. E., and Ruedy, R.: MATRIX (Multiconfiguration Aerosol TRacker of mIXing state): an aerosol microphysical module for global atmospheric models, *Atmos. Chem. Phys.*, 8, 6003–6035, doi:10.5194/acp-8-6003-2008, 2008.

Bian, H. S. and Prather, M. J.: Fast-J2: accurate simulation of stratospheric photolysis in global chemical models, *J. Atmos. Chem.*, 41, 281–296, doi:10.1023/a:1014980619462, 2002.

Boucher, O., Randall, D., Artaxo, P., Bretherton, C., Feingold, G., Forster, P., Kerminen, V.-M., Kondo, Y., Liao, H., Lohmann, U., Rasch, P., Satheesh, S. K., Sherwood, S., Stevens, B., and Zhang, X. Y.: Clouds and aerosols, in: Climate Change 2013: the Physical Science Basis, Contribution of Working Group I to the Fifth Assessment Report of the Intergovernmental Panel on Climate Change, Cambridge University Press, Cambridge, UK and New York, NY, USA, 571–657, 2013.

Bowman, K. W., Shindell, D. T., Worden, H. M., Lamarque, J. F., Young, P. J., Stevenson, D. S., Qu, Z., de la Torre, M., Bergmann, D., Cameron-Smith, P. J., Collins, W. J., Doherty, R., Dalsøren, S. B., Faluvegi, G., Folberth, G., Horowitz, L. W., Josse, B. M., Lee, Y. H., MacKenzie, I. A., Myhre, G., Nagashima, T., Naik, V., Plummer, D. A., Rumbold, S. T., Skeie, R. B., Strode, S. A., Sudo, K., Szopa, S., Voulgarakis, A., Zeng, G., Kulawik, S. S., Aghedo, A. M., and Worden, J. R.: Evaluation of ACCMIP outgoing longwave radiation from tropospheric ozone using TES satellite observations, *Atmos. Chem. Phys.*, 13, 4057–4072, doi:10.5194/acp-13-4057-2013, 2013.

Cakmur, R. V., Miller, R. L., Perlitz, J., Geogdzhayev, I. V., Ginoux, P., Koch, D., Kohfeld, K. E., Tegen, I., and Zender, C. S.: Constraining the magnitude of the global dust cycle by min-

ModelE2-TOMAS: global aerosol microphysics model

Y. H. Lee et al.

[Title Page](#)

[Abstract](#)

[Introduction](#)

[Conclusions](#)

[References](#)

[Tables](#)

[Figures](#)



[Back](#)

[Close](#)

[Full Screen / Esc](#)

[Printer-friendly Version](#)

[Interactive Discussion](#)



scription and evaluation of aerosols and trace gases, *J. Geophys. Res.-Atmos.*, 109, doi:10.1029/2004JD004571, 2004.

Emmons, L. K., Hauglustaine, D. A., Muller, J. F., Carroll, M. A., Brasseur, G. P., Brunner, D., Staehelin, J., Thouret, V., and Marenco, A.: Data composites of airborne observations of tropospheric ozone and its precursors, *J. Geophys. Res.-Atmos.*, 105, 20497–20538, doi:10.1029/2000jd900232, 2000.

Forster, P. and Ramaswamy, V.: Changes in atmospheric constituents and in radiative forcing, in: *Climate Change 2007: The Physical Science Basis*, edited by: Solomon, S., Qin, D., Manning, M., Marquis, M., Averyt, K., Tignor, M. M. B., Miller, H. L., and Chen, Z. L., 129–234, 2007.

Ginoux, P., Chin, M., Tegen, I., Prospero, J. M., Holben, B., Dubovik, O., and Lin, S. J.: Sources and distributions of dust aerosols simulated with the GOCART model, *J. Geophys. Res.-Atmos.*, 106, 20255–20273, 2001.

Gong, S. L.: A parameterization of sea-salt aerosol source function for sub- and super-micron particles, *Global Biogeochem. Cy.*, 17, 1097, doi:10.1029/2003gb002079, 2003.

Hand, J. L., Copeland, S. A., Day, D. E., Dillner, A. M., Indresand, H., Malm, W. C., McDade, C. E., Moore, C. T., Pitchford, M. L., Schichtel, B. A., and Watson, J. G.: Spatial and Seasonal Patterns and Temporal Variability of Haze and its Constituents in the United States: Report V, Colo. State Univ., Fort Collins, 2011.

Hansen, J., Russell, G., Rind, D., Stone, P., Lacis, A., Lebedeff, S., Ruedy, R., and Travis, L.: Efficient 3-dimensional global-models for climate studies – Model-I and Model-II, *Mon. Weather Rev.*, 111, 609–662, 1983.

Heintzenberg, J., Covert, D. C., and Van Dingenen, R.: Size distribution and chemical composition of marine aerosols: a compilation and review, *Tellus B*, 52, 1104–1122, doi:10.1034/j.1600-0889.2000.00136.x, 2000.

Hoell, J. M., Davis, D. D., Jacob, D. J., Rodgers, M. O., Newell, R. E., Fuelberg, H. E., McNeal, R. J., Raper, J. L., and Bendura, R. J.: Pacific Exploratory Mission in the tropical Pacific: PEM-Tropics A, August–September 1996, *J. Geophys. Res.-Atmos.*, 104, 5567–5583, doi:10.1029/1998jd100074, 1999.

Holben, B. N., Eck, T. F., Slutsker, I., Tanre, D., Buis, J. P., Setzer, A., Vermote, E., Reagan, J. A., Kaufman, Y. J., Nakajima, T., Lavenu, F., Jankowiak, I., and Smirnov, A.: AERONET – a federated instrument network and data archive for aerosol characterization, *Remote Sens. Environ.*, 66, 1–16, doi:10.1016/s0034-4257(98)00031-5, 1998.

[Title Page](#)[Abstract](#)[Introduction](#)[Conclusions](#)[References](#)[Tables](#)[Figures](#)[◀](#)[▶](#)[◀](#)[▶](#)[Back](#)[Close](#)[Full Screen / Esc](#)[Printer-friendly Version](#)[Interactive Discussion](#)

Title Page	
Abstract	Introduction
Conclusions	References
Tables	Figures
Full Screen / Esc	
Printer-friendly Version	
Interactive Discussion	



- Holben, B. N., Tanre, D., Smirnov, A., Eck, T. F., Slutsker, I., Abuhassan, N., Newcomb, W. W., Schafer, J. S., Chatenet, B., Lavenue, F., Kaufman, Y. J., Castle, J. V., Setzer, A., Markham, B., Clark, D., Frouin, R., Halthore, R., Karneli, A., O'Neill, N. T., Pietras, C., Pinker, R. T., Voss, K., and Zibordi, G.: An emerging ground-based aerosol climatology: aerosol optical depth from AERONET, *J. Geophys. Res.-Atmos.*, 106, 12067–12097, doi:10.1029/2001jd900014, 2001.
- Hsu, N. C., Tsay, S. C., King, M. D., and Herman, J. R.: Deep blue retrievals of Asian aerosol properties during ACE-Asia, *IEEE T. Geosci. Remote*, 44, 3180–3195, doi:10.1109/tgrs.2006.879540, 2006.
- Jourdain, B. and Legrand, M.: Seasonal variations of atmospheric dimethylsulfide, dimethylsulfoxide, sulfur dioxide, methanesulfonate, and non-sea-salt sulfate aerosols at Dumont d'Urville (coastal Antarctica) (December 1998 to July 1999), *J. Geophys. Res.-Atmos.*, 106, 14391–14408, doi:10.1029/2000jd900841, 2001.
- Jung, J. G., Adams, P. J., and Pandis, S. N.: Simulating the size distribution and chemical composition of ultrafine particles during nucleation events, *Atmos. Environ.*, 40, 2248–2259, 2006.
- Jung, J. G., Fountoukis, C., Adams, P. J., and Pandis, S. N.: Simulation of in situ ultrafine particle formation in the eastern United States using PMCAMx-UF, *J. Geophys. Res.-Atmos.*, 115, D03203, doi:10.1029/2009jd012313, 2010.
- Kahn, R. A., Gaitley, B. J., Martonchik, J. V., Diner, D. J., Crean, K. A., and Holben, B.: Multiangle Imaging Spectroradiometer (MISR) global aerosol optical depth validation based on 2 years of coincident Aerosol Robotic Network (AERONET) observations, *J. Geophys. Res.-Atmos.*, 110, D10s04, doi:10.1029/2004jd004706, 2005.
- Kettle, A. J. and Andreae, M. O.: Flux of dimethylsulfide from the oceans: a comparison of updated data sets and flux models, *J. Geophys. Res.-Atmos.*, 105, 26793–26808, doi:10.1029/2000JD900252, 2000.
- Kettle, A. J., Andreae, M. O., Amouroux, D., Andreae, T. W., Bates, T. S., Berresheim, H., Bingermer, H., Boniforti, R., Curran, M. A. J., DiTullio, G. R., Helas, G., Jones, G. B., Keller, M. D., Kiene, R. P., Leck, C., Levasseur, M., Malin, G., Maspero, M., Matrai, P., McTaggart, A. R., Mihalopoulos, N., Nguyen, B. C., Novo, A., Putaud, J. P., Rapsomanikis, S., Roberts, G., Schebeske, G., Sharma, S., Simo, R., Staubes, R., Turner, S., and Uher, G.: A global database of sea surface dimethylsulfide (DMS) measurements and a procedure to predict sea surface DMS as a function of latitude, longitude, and month, *Global Biogeochem. Cy.*, 13, 399–444, doi:10.1029/1999gb900004, 1999.

[Title Page](#)

[Abstract](#)

[Introduction](#)

[Conclusions](#)

[References](#)

[Tables](#)

[Figures](#)

◀

▶

◀

▶

[Back](#)

[Close](#)

[Full Screen / Esc](#)

[Printer-friendly Version](#)

[Interactive Discussion](#)



Koch, D., Jacob, D., Tegen, I., Rind, D., and Chin, M.: Tropospheric sulfur simulation and sulfate direct radiative forcing in the Goddard Institute for Space Studies general circulation model, *J. Geophys. Res.-Atmos.*, 104, 23799–23822, doi:10.1029/1999jd900248, 1999.

Koch, D., Schmidt, G. A., and Field, C. V.: Sulfur, sea salt, and radionuclide aerosols in GISS ModelE, *J. Geophys. Res.-Atmos.*, 111, D06206, doi:10.1029/2004jd005550, 2006.

Koch, D., Bond, T. C., Streets, D., Unger, N., and van der Werf, G. R.: Global impacts of aerosols from particular source regions and sectors, *J. Geophys. Res.-Atmos.*, 112, D02205, doi:10.1029/2005jd007024, 2007.

Koch, D., Bauer, S. E., Del Genio, A., Faluvegi, G., McConnell, J. R., Menon, S., Miller, R. L., Rind, D., Ruedy, R., Schmidt, G. A., and Shindell, D.: Coupled aerosol-chemistry-climate twentieth-century transient model investigation: trends in short-lived species and climate responses, *J. Climate*, 24, 2693–2714, doi:10.1175/2011jcli3582.1, 2011.

Korhonen, H., Carslaw, K. S., Spracklen, D. V., Mann, G. W., and Woodhouse, M. T.: Influence of oceanic dimethyl sulfide emissions on cloud condensation nuclei concentrations and seasonality over the remote Southern Hemisphere oceans: a global model study, *J. Geophys. Res.-Atmos.*, 113, D15204, doi:10.1029/2007jd009718, 2008.

Lamarque, J.-F., Dentener, F., McConnell, J., Ro, C.-U., Shaw, M., Vet, R., Bergmann, D., Cameron-Smith, P., Dalsoren, S., Doherty, R., Faluvegi, G., Ghan, S. J., Josse, B., Lee, Y. H., MacKenzie, I. A., Plummer, D., Shindell, D. T., Skeie, R. B., Stevenson, D. S., Strode, S., Zeng, G., Curran, M., Dahl-Jensen, D., Das, S., Fritzsche, D., and Nolan, M.: Multi-model mean nitrogen and sulfur deposition from the Atmospheric Chemistry and Climate Model Intercomparison Project (ACCMIP): evaluation of historical and projected future changes, *Atmos. Chem. Phys.*, 13, 7997–8018, doi:10.5194/acp-13-7997-2013, 2013a.

Lamarque, J.-F., Shindell, D. T., Josse, B., Young, P. J., Cionni, I., Eyring, V., Bergmann, D., Cameron-Smith, P., Collins, W. J., Doherty, R., Dalsoren, S., Faluvegi, G., Folberth, G., Ghan, S. J., Horowitz, L. W., Lee, Y. H., MacKenzie, I. A., Nagashima, T., Naik, V., Plummer, D., Righi, M., Rumbold, S. T., Schulz, M., Skeie, R. B., Stevenson, D. S., Strode, S., Sudo, K., Szopa, S., Voulgarakis, A., and Zeng, G.: The Atmospheric Chemistry and Climate Model Intercomparison Project (ACCMIP): overview and description of models, simulations and climate diagnostics, *Geosci. Model Dev.*, 6, 179–206, doi:10.5194/gmd-6-179-2013, 2013b.

Title Page	
Abstract	Introduction
Conclusions	References
Tables	Figures
Full Screen / Esc	
Printer-friendly Version	
Interactive Discussion	

- Lauer, A., Hendricks, J., Ackermann, I., Schell, B., Hass, H., and Metzger, S.: Simulating aerosol microphysics with the ECHAM/MADE GCM – Part I: Model description and comparison with observations, *Atmos. Chem. Phys.*, 5, 3251–3276, doi:10.5194/acp-5-3251-2005, 2005.
- Lee, Y. H. and Adams, P. J.: Evaluation of aerosol distributions in the GISS-TOMAS global aerosol microphysics model with remote sensing observations, *Atmos. Chem. Phys.*, 10, 2129–2144, doi:10.5194/acp-10-2129-2010, 2010.
- Lee, Y. H. and Adams, P. J.: A fast and efficient version of the Two-Moment Aerosol Sectional (TOMAS) global aerosol microphysics model, *Aerosol Sci. Tech.*, 46, 678–689, doi:10.1080/02786826.2011.643259, 2012.
- Lee, Y. H., Chen, K., and Adams, P. J.: Development of a global model of mineral dust aerosol microphysics, *Atmos. Chem. Phys.*, 9, 2441–2458, doi:10.5194/acp-9-2441-2009, 2009.
- Lee, Y. H., Lamarque, J.-F., Flanner, M. G., Jiao, C., Shindell, D. T., Berntsen, T., Bisiaux, M. M., Cao, J., Collins, W. J., Curran, M., Edwards, R., Faluvegi, G., Ghan, S., Horowitz, L. W., McConnell, J. R., Ming, J., Myhre, G., Nagashima, T., Naik, V., Rumbold, S. T., Skeie, R. B., Sudo, K., Takemura, T., Thevenon, F., Xu, B., and Yoon, J.-H.: Evaluation of preindustrial to present-day black carbon and its albedo forcing from Atmospheric Chemistry and Climate Model Intercomparison Project (ACCMIP), *Atmos. Chem. Phys.*, 13, 2607–2634, doi:10.5194/acp-13-2607-2013, 2013a.
- Lee, Y. H., Pierce, J. R., and Adams, P. J.: Representation of nucleation mode microphysics in a global aerosol model with sectional microphysics, *Geosci. Model Dev.*, 6, 1221–1232, doi:10.5194/gmd-6-1221-2013, 2013b.
- Liss, P. S. and Merlivat, L.: Air-sea gas exchange rates: introduction and synthesis, in: *The Role of Air-Sea Exchange in Geochemical Cycling*, Springer, New York, 1986.
- Liu, X. H., Penner, J. E., and Herzog, M.: Global modeling of aerosol dynamics: model description, evaluation, and interactions between sulfate and nonsulfate aerosols, *J. Geophys. Res.-Atmos.*, 110, D18206, doi:10.1029/2004jd005674, 2005.
- Lohmann, U. and Feichter, J.: Global indirect aerosol effects: a review, *Atmos. Chem. Phys.*, 5, 715–737, doi:10.5194/acp-5-715-2005, 2005.
- Mahowald, N. M., Engelstaedter, S., Luo, C., Sealy, A., Artaxo, P., Benitez-Nelson, C., Bonnet, S., Chen, Y., Chuang, P. Y., Cohen, D. D., Dulac, F., Herut, B., Johansen, A. M., Kubilay, N., Losno, R., Maenhaut, W., Paytan, A., Prospero, J. A., Shank, L. M., and Siefert, R. L.: Atmospheric iron deposition: global distribution, variability, and human perturbations, *Annu. Rev. Mar. Sci.*, 245–278, 2009.



- Mann, G. W., Carslaw, K. S., Spracklen, D. V., Ridley, D. A., Manktelow, P. T., Chipperfield, M. P., Pickering, S. J., and Johnson, C. E.: Description and evaluation of GLOMAP-mode: a modal global aerosol microphysics model for the UKCA composition-climate model, *Geosci. Model Dev.*, 3, 519–551, doi:10.5194/gmd-3-519-2010, 2010.
- 5 Menon, S., Del Genio, A. D., Koch, D., and Tselioudis, G.: GCM Simulations of the aerosol indirect effect: sensitivity to cloud parameterization and aerosol burden, *J. Atmos. Sci.*, 59, 692–713, doi:10.1175/1520-0469(2002)059<0692:gsotai>2.0.co;2, 2002.
- 10 Menon, S., Del Genio, A. D., Kaufman, Y., Bennartz, R., Koch, D., Loeb, N., and Orlikowski, D.: Analyzing signatures of aerosol-cloud interactions from satellite retrievals and the GISS GCM to constrain the aerosol indirect effect, *J. Geophys. Res.-Atmos.*, 113, D14s22, doi:10.1029/2007jd009442, 2008.
- Merikanto, J., Spracklen, D. V., Mann, G. W., Pickering, S. J., and Carslaw, K. S.: Impact of nucleation on global CCN, *Atmos. Chem. Phys.*, 9, 8601–8616, doi:10.5194/acp-9-8601-2009, 2009.
- 15 Miller, R. L., Cakmur, R. V., Perlitz, J., Geogdzhayev, I. V., Ginoux, P., Koch, D., Kohfeld, K. E., Prigent, C., Ruedy, R., Schmidt, G. A., and Tegen, I.: Mineral dust aerosols in the NASA goddard institute for Space Sciences ModelE atmospheric general circulation model, *J. Geophys. Res.-Atmos.*, 111, D06208, doi:10.1029/2005jd005796, 2006.
- 20 Mishchenko, M. I., Travis, L. D., and Mackowski, D. W.: T-matrix computations of light scattering by nonspherical particles: a review, *J. Quant. Spectrosc. Ra.*, 55, 535–575, doi:10.1016/0022-4073(96)00002-7, 1996.
- Monahan, E. C., Spiel, D. E., and David, K. L.: A model of marine aerosol generation via white-caps and wave disruption, in: Oceanic Whitecaps, edited by: Monahan, E. C. and Mac Nio-25 caill, G., Oceanographic Sciences Library, 167–174, 1986.
- Myhre, G., Samset, B. H., Schulz, M., Balkanski, Y., Bauer, S., Berntsen, T. K., Bian, H., Bellouin, N., Chin, M., Diehl, T., Easter, R. C., Feichter, J., Ghan, S. J., Hauglustaine, D., Iversen, T., Kinne, S., Kirkevåg, A., Lamarque, J.-F., Lin, G., Liu, X., Lund, M. T., Luo, G., Ma, X., van Noije, T., Penner, J. E., Rasch, P. J., Ruiz, A., Seland, Ø., Skeie, R. B., Stier, P., Takemura, T., Tsigaridis, K., Wang, P., Wang, Z., Xu, L., Yu, H., Yu, F., Yoon, J.-H., Zhang, K., Zhang, H., and Zhou, C.: Radiative forcing of the direct aerosol effect from AeroCom Phase II simulations, *Atmos. Chem. Phys.*, 13, 1853–1877, doi:10.5194/acp-13-1853-2013, 2013a.
- 30 Myhre, G., Shindell, D., Bréon, F.-M., Collins, W., Fuglestvedt, J., Huang, J., Koch, D., Lamarque, J. F., Lee, D., Mendoza, B., Nakajima, T., Robock, A., Stephens, G., Takemura, T., and

ModelE2-TOMAS: global aerosol microphysics model

Y. H. Lee et al.

[Title Page](#)

[Abstract](#)

[Introduction](#)

[Conclusions](#)

[References](#)

[Tables](#)

[Figures](#)



[Back](#)

[Close](#)

[Full Screen / Esc](#)

[Printer-friendly Version](#)

[Interactive Discussion](#)



[Title Page](#)

[Abstract](#)

[Introduction](#)

[Conclusions](#)

[References](#)

[Tables](#)

[Figures](#)



[Back](#)

[Close](#)

[Full Screen / Esc](#)

[Printer-friendly Version](#)

[Interactive Discussion](#)



Zhang, H.: Anthropogenic and natural radiative forcing, in: Climate Change 2013: The Physical Science Basis, Contribution of Working Group I to the Fifth Assessment Report of the Intergovernmental Panel on Climate Change, Cambridge University Press, Cambridge, UK and New York, NY, USA, 2013b.

Nabat, P., Somot, S., Mallet, M., Chiapello, I., Morcrette, J. J., Solmon, F., Szopa, S., Dulac, F., Collins, W., Ghan, S., Horowitz, L. W., Lamarque, J. F., Lee, Y. H., Naik, V., Nagashima, T., Shindell, D., and Skeie, R.: A 4-D climatology (1979–2009) of the monthly tropospheric aerosol optical depth distribution over the Mediterranean region from a comparative evaluation and blending of remote sensing and model products, *Atmos. Meas. Tech.*, 6, 1287–1314, doi:10.5194/amt-6-1287-2013, 2013.

Naik, V., Voulgarakis, A., Fiore, A. M., Horowitz, L. W., Lamarque, J.-F., Lin, M., Prather, M. J., Young, P. J., Bergmann, D., Cameron-Smith, P. J., Cionni, I., Collins, W. J., Dalsøren, S. B., Doherty, R., Eyring, V., Faluvegi, G., Folberth, G. A., Josse, B., Lee, Y. H., MacKenzie, I. A., Nagashima, T., van Noije, T. P. C., Plummer, D. A., Righi, M., Rumbold, S. T., Skeie, R., Shindell, D. T., Stevenson, D. S., Strode, S., Sudo, K., Szopa, S., and Zeng, G.: Preindustrial to present-day changes in tropospheric hydroxyl radical and methane lifetime from the Atmospheric Chemistry and Climate Model Intercomparison Project (ACCMIP), *Atmos. Chem. Phys.*, 13, 5277–5298, doi:10.5194/acp-13-5277-2013, 2013.

Napari, I., Noppel, M., Vehkamaki, H., and Kulmala, M.: Parametrization of ternary nucleation rates for $\text{H}_2\text{SO}_4\text{-NH}_3\text{-H}_2\text{O}$ vapors, *J. Geophys. Res.-Atmos.*, 107, 4381, doi:10.1029/2002JD002132, 2002.

Nguyen, B. C., Mihalopoulos, N., Putaud, J. P., Gaudry, A., Gallet, L., Keene, W. C., and Galloway, J. N.: Covariations in oceanic dimethyl sulfide, its oxidation-products and rain acidity at Amsterdam Island in the southern Indian-Ocean, *J. Atmos. Chem.*, 15, 39–53, doi:10.1007/bf00053608, 1992.

Nightingale, P. D., Malin, G., Law, C. S., Watson, A. J., Liss, P. S., Liddicoat, M. I., Boutin, J., and Upstill-Goddard, R. C.: In situ evaluation of air-sea gas exchange parameterizations using novel conservative and volatile tracers, *Global Biogeochem. Cy.*, 14, 373–387, doi:10.1029/1999gb900091, 2000.

Petzold, A., Fiebig, M., Flentje, H., Keil, A., Leiterer, U., Schroder, F., Stifter, A., Wendisch, M., and Wendling, P.: Vertical variability of aerosol properties observed at a continental site during the Lindenberg Aerosol Characterization Experiment (LACE 98), *J. Geophys. Res.-Atmos.*, 107, 8128, doi:10.1029/2001jd001043, 2002.

- Pierce, J. R. and Adams, P. J.: Global evaluation of CCN formation by direct emission of sea salt and growth of ultrafine sea salt, *J. Geophys. Res.-Atmos.*, 111, D06203, doi:10.1029/2005JD006186, 2006.
- Pierce, J. R. and Adams, P. J.: Uncertainty in global CCN concentrations from uncertain aerosol nucleation and primary emission rates, *Atmos. Chem. Phys.*, 9, 1339–1356, doi:10.5194/acp-9-1339-2009, 2009a.
- Pierce, J. R. and Adams, P. J.: A computationally efficient aerosol nucleation/condensation method: pseudo-steady-state sulfuric acid, *Aerosol Sci. Tech.*, 43, 216–226, 2009b.
- Pierce, J. R., Chen, K., and Adams, P. J.: Contribution of primary carbonaceous aerosol to cloud condensation nuclei: processes and uncertainties evaluated with a global aerosol microphysics model, *Atmos. Chem. Phys.*, 7, 5447–5466, doi:10.5194/acp-7-5447-2007, 2007.
- Prospero, J. M. and Bonatti, E.: Continental dust in atmosphere of eastern equatorial Pacific, *J. Geophys. Res.*, 74, 3362–3371, doi:10.1029/JC074i013p03362, 1969.
- Putaud, J. P., Van Dingenen, R., Alastuey, A., Bauer, H., Birmili, W., Cyrys, J., Flentje, H., Fuzzi, S., Gehrig, R., Hansson, H. C., Harrison, R. M., Herrmann, H., Hitzenberger, R., Hueglin, C., Jones, A. M., Kasper-Giebl, A., Kiss, G., Kousa, A., Kuhlbusch, T. A. J., Loeschau, G., Maenhaut, W., Molnar, A., Moreno, T., Pekkanen, J., Perrino, C., Pitz, M., Puxbaum, H., Querol, X., Rodriguez, S., Salma, I., Schwarz, J., Smolik, J., Schneider, J., Spindler, G., ten Brink, H., Tursic, J., Viana, M., Wiedensohler, A., and Raes, F.: A European aerosol phenomenology-3: physical and chemical characteristics of particulate matter from 60 rural, urban, and kerbside sites across Europe, *Atmos. Environ.*, 44, 1308–1320, doi:10.1016/j.atmosenv.2009.12.011, 2010.
- Raper, J. L., Kleb, M. M., Jacob, D. J., Davis, D. D., Newell, R. E., Fuelberg, H. E., Benndura, R. J., Hoell, J. M., and McNeal, R. J.: Pacific Exploratory Mission in the tropical Pacific: PEM-Tropics B, March–April 1999, *J. Geophys. Res.-Atmos.*, 106, 32401–32425, doi:10.1029/2000jd900833, 2001.
- Remer, L. A., Kleidman, R. G., Levy, R. C., Kaufman, Y. J., Tanre, D., Mattoo, S., Martins, J. V., Ichoku, C., Koren, I., Yu, H., and Holben, B. N.: Global aerosol climatology from the MODIS satellite sensors, *J. Geophys. Res.-Atmos.*, 113, D14s07, doi:10.1029/2007jd009661, 2008.
- Savoie, D. L. and Prospero, J. M.: Comparison of oceanic and continental sources of non-sea-salt sulfate over the Pacific-Ocean, *Nature*, 339, 685–687, doi:10.1038/339685a0, 1989.
- Schmidt, G. A., Ruedy, R., Hansen, J. E., Aleinov, I., Bell, N., Bauer, M., Bauer, S., Cairns, B., Canuto, V., Cheng, Y., Del Genio, A., Faluvegi, G., Friend, A. D., Hall, T. M., Hu, Y. Y., Kel-

ModelE2-TOMAS:
global aerosol
microphysics model

Y. H. Lee et al.

[Title Page](#)

[Abstract](#)

[Introduction](#)

[Conclusions](#)

[References](#)

[Tables](#)

[Figures](#)



[Back](#)

[Close](#)

[Full Screen / Esc](#)

[Printer-friendly Version](#)

[Interactive Discussion](#)



ley, M., Kiang, N. Y., Koch, D., Lacis, A. A., Lerner, J., Lo, K. K., Miller, R. L., Nazarenko, L., Oinas, V., Perlitz, J., Perlitz, J., Rind, D., Romanou, A., Russell, G. L., Sato, M., Shindell, D. T., Stone, P. H., Sun, S., Tausnev, N., Thresher, D., and Yao, M. S.: Present-day atmospheric simulations using GISS ModelE: comparison to in situ, satellite, and reanalysis data, *J. Climate*, 19, 153–192, doi:10.1175/jcli3612.1, 2006.

5 Schmidt, G. A., Kelley, M., Nazarenko, L., Ruedy, R., Russell, G. L., Aleinov, I., Bauer, M., Bauer, S. E., Bhat, M. K., Bleck, R., Canuto, V., Chen, Y.-H., Cheng, Y., Clune, T. L., Del Genio, A., de Fainchtein, R., Faluvegi, G., Hansen, J. E., Healy, R. J., Kiang, N. Y., Koch, D., Lacis, A. A., LeGrande, A. N., Lerner, J., Lo, K. K., Matthews, E. E., Menon, S., Miller, R. L., Oinas, V., Oloso, A. O., Perlitz, J. P., Puma, M. J., Putman, W. M., Rind, D., Romanou, A., Sato, M., Shindell, D. T., Sun, S., Syed, R. A., Tausnev, N., Tsigaridis, K., Unger, N., Voulgarakis, A., Yao, M.-S., and Zhang, J.: Configuration and assessment of the GISS ModelE2 contributions to the CMIP5 archive, *J. Adv. Model. Earth Syst.*, 6, 141–184, doi:10.1002/2013ms000265, 2014.

10 Seinfeld, J. H. and Pandis, S. N.: *Atmospheric Chemistry and Physics*, John Wiley and Sons, New York, 1998.

15 Shindell, D. T., Faluvegi, G., Unger, N., Aguilar, E., Schmidt, G. A., Koch, D. M., Bauer, S. E., and Miller, R. L.: Simulations of preindustrial, present-day, and 2100 conditions in the NASA GISS composition and climate model G-PUCCINI, *Atmos. Chem. Phys.*, 6, 4427–4459, doi:10.5194/acp-6-4427-2006, 2006.

20 Shindell, D., Faluvegi, G., Walsh, M., Anenberg, S. C., Van Dingenen, R., Muller, N. Z., Austin, J., Koch, D., and Milly, G.: Climate, health, agricultural and economic impacts of tighter vehicle-emission standards, *Nature Climate Change*, 1, 59–66, doi:10.1038/nclimate1066, 2011.

25 Shindell, D. T., Lamarque, J.-F., Schulz, M., Flanner, M., Jiao, C., Chin, M., Young, P. J., Lee, Y. H., Rotstyn, L., Mahowald, N., Milly, G., Faluvegi, G., Balkanski, Y., Collins, W. J., Conley, A. J., Dalsoren, S., Easter, R., Ghan, S., Horowitz, L., Liu, X., Myhre, G., Naganashima, T., Naik, V., Rumbold, S. T., Skeie, R., Sudo, K., Szopa, S., Takemura, T., Voulgarakis, A., Yoon, J.-H., and Lo, F.: Radiative forcing in the ACCMIP historical and future climate simulations, *Atmos. Chem. Phys.*, 13, 2939–2974, doi:10.5194/acp-13-2939-2013, 2013.

30 Sihto, S.-L., Kulmala, M., Kerminen, V.-M., Dal Maso, M., Petäjä, T., Riipinen, I., Korhonen, H., Arnold, F., Janson, R., Boy, M., Laaksonen, A., and Lehtinen, K. E. J.: Atmospheric sul-

ModelE2-TOMAS: global aerosol microphysics model

Y. H. Lee et al.

[Title Page](#)

[Abstract](#)

[Introduction](#)

[Conclusions](#)

[References](#)

[Tables](#)

[Figures](#)



[Back](#)

[Close](#)

[Full Screen / Esc](#)

[Printer-friendly Version](#)

[Interactive Discussion](#)



phuric acid and aerosol formation: implications from atmospheric measurements for nucleation and early growth mechanisms, *Atmos. Chem. Phys.*, 6, 4079–4091, doi:10.5194/acp-6-4079-2006, 2006.

5 Singh, S., Adams, P. J., Misquitta, A., Lee, K. J., Lipsky, E. M., and Robinson, A. L.: Computational analysis of particle nucleation in dilution tunnels: effects of flow configuration and tunnel geometry, *Aerosol Sci. Tech.*, 48, 638–648, doi:10.1080/02786826.2014.910291, 2014.

10 Spracklen, D. V., Pringle, K. J., Carslaw, K. S., Chipperfield, M. P., and Mann, G. W.: A global off-line model of size-resolved aerosol microphysics: I. Model development and prediction of aerosol properties, *Atmos. Chem. Phys.*, 5, 2227–2252, doi:10.5194/acp-5-2227-2005, 2005.

15 Spracklen, D. V., Carslaw, K. S., Merikanto, J., Mann, G. W., Reddington, C. L., Pickering, S., Ogren, J. A., Andrews, E., Baltensperger, U., Weingartner, E., Boy, M., Kulmala, M., Laakso, L., Lihavainen, H., Kivekäs, N., Komppula, M., Mihalopoulos, N., Kouvarakis, G., Jennings, S. G., O'Dowd, C., Birmili, W., Wiedensohler, A., Weller, R., Gras, J., Laj, P., Sellegrí, K., Bonn, B., Krejci, R., Laaksonen, A., Hamed, A., Minikin, A., Harrison, R. M., Talbot, R., and Sun, J.: Explaining global surface aerosol number concentrations in terms of primary emissions and particle formation, *Atmos. Chem. Phys.*, 10, 4775–4793, doi:10.5194/acp-10-4775-2010, 2010.

20 Spracklen, D. V., Carslaw, K. S., Pöschl, U., Rap, A., and Forster, P. M.: Global cloud condensation nuclei influenced by carbonaceous combustion aerosol, *Atmos. Chem. Phys.*, 11, 9067–9087, doi:10.5194/acp-11-9067-2011, 2011.

25 Stevens, R. G., Pierce, J. R., Brock, C. A., Reed, M. K., Crawford, J. H., Holloway, J. S., Ryerson, T. B., Huey, L. G., and Nowak, J. B.: Nucleation and growth of sulfate aerosol in coal-fired power plant plumes: sensitivity to background aerosol and meteorology, *Atmos. Chem. Phys.*, 12, 189–206, doi:10.5194/acp-12-189-2012, 2012.

30 Stevenson, D. S., Young, P. J., Naik, V., Lamarque, J.-F., Shindell, D. T., Voulgarakis, A., Skeie, R. B., Dalsoren, S. B., Myhre, G., Berntsen, T. K., Folberth, G. A., Rumbold, S. T., Collins, W. J., MacKenzie, I. A., Doherty, R. M., Zeng, G., van Noije, T. P. C., Strunk, A., Bergmann, D., Cameron-Smith, P., Plummer, D. A., Strode, S. A., Horowitz, L., Lee, Y. H., Szopa, S., Sudo, K., Nagashima, T., Josse, B., Cionni, I., Righi, M., Eyring, V., Conley, A., Bowman, K. W., Wild, O., and Archibald, A.: Tropospheric ozone changes, radiative forcing and attribution to emissions in the Atmospheric Chemistry and Climate Model Intercom-

[Title Page](#)[Abstract](#)[Introduction](#)[Conclusions](#)[References](#)[Tables](#)[Figures](#)[Back](#)[Close](#)[Full Screen / Esc](#)[Printer-friendly Version](#)[Interactive Discussion](#)

ModelE2-TOMAS: global aerosol microphysics model

Y. H. Lee et al.

[Title Page](#)

[Abstract](#)

[Introduction](#)

[Conclusions](#)

[References](#)

[Tables](#)

[Figures](#)



[Back](#)

[Close](#)

[Full Screen / Esc](#)

[Printer-friendly Version](#)

[Interactive Discussion](#)



- Uematsu, M., Duce, R. A., and Prospero, J. M.: Deposition of atmospheric mineral particles in the north Pacific-Ocean, *J. Atmos. Chem.*, 3, 123–138, doi:10.1007/bf00049372, 1985.
- van der Werf, G. R., Randerson, J. T., Giglio, L., Collatz, G. J., Mu, M., Kasibhatla, P. S., Morton, D. C., DeFries, R. S., Jin, Y., and van Leeuwen, T. T.: Global fire emissions and the contribution of deforestation, savanna, forest, agricultural, and peat fires (1997–2009), *Atmos. Chem. Phys.*, 10, 11707–11735, doi:10.5194/acp-10-11707-2010, 2010.
- Vehkamaki, H., Kulmala, M., Napari, I., Lehtinen, K. E. J., Timmreck, C., Noppel, M., and Laaksonen, A.: An improved parameterization for sulfuric acid-water nucleation rates for tropospheric and stratospheric conditions, *J. Geophys. Res.-Atmos.*, 107, 4622, doi:10.1029/2002JD002184, 2002.
- Vignati, E., Wilson, J., and Stier, P.: M7: An efficient size-resolved aerosol microphysics module for large-scale aerosol transport models, *J. Geophys. Res.-Atmos.*, 109, D22202, doi:10.1029/2003jd004485, doi:10.1029/2003jd004485, 2004.
- Wang, M., Ghan, S., Ovchinnikov, M., Liu, X., Easter, R., Kassianov, E., Qian, Y., and Morrison, H.: Aerosol indirect effects in a multi-scale aerosol-climate model PNNL-MMF, *Atmos. Chem. Phys.*, 11, 5431–5455, doi:10.5194/acp-11-5431-2011, 2011.
- Wanninkhof, R.: Relationship between wind speed and gas exchange over the ocean, *J. Geophys. Res.-Oceans*, 97, 7373–7382, doi:10.1029/92jc00188, 1992.
- Westervelt, D. M., Pierce, J. R., Riipinen, I., Trivitayanurak, W., Hamed, A., Kulmala, M., Laaksonen, A., Decesari, S., and Adams, P. J.: Formation and growth of nucleated particles into cloud condensation nuclei: model–measurement comparison, *Atmos. Chem. Phys.*, 13, 7645–7663, doi:10.5194/acp-13-7645-2013, 2013.
- Young, P. J., Archibald, A. T., Bowman, K. W., Lamarque, J.-F., Naik, V., Stevenson, D. S., Tilmes, S., Voulgarakis, A., Wild, O., Bergmann, D., Cameron-Smith, P., Cionni, I., Collins, W. J., Dalsøren, S. B., Doherty, R. M., Eyring, V., Faluvegi, G., Horowitz, L. W., Josse, B., Lee, Y. H., MacKenzie, I. A., Nagashima, T., Plummer, D. A., Righi, M., Rumbold, S. T., Skeie, R. B., Shindell, D. T., Strode, S. A., Sudo, K., Szopa, S., and Zeng, G.: Pre-industrial to end 21st century projections of tropospheric ozone from the Atmospheric Chemistry and Climate Model Intercomparison Project (ACCMIP), *Atmos. Chem. Phys.*, 13, 2063–2090, doi:10.5194/acp-13-2063-2013, 2013.
- Yu, F. and Luo, G.: Simulation of particle size distribution with a global aerosol model: contribution of nucleation to aerosol and CCN number concentrations, *Atmos. Chem. Phys.*, 9, 7691–7710, doi:10.5194/acp-9-7691-2009, 2009.

Title Page	
Abstract	Introduction
Conclusions	References
Tables	Figures
◀◀	▶▶
◀	▶
Back	Close
Full Screen / Esc	
Printer-friendly Version	
Interactive Discussion	



**ModelE2-TOMAS:
global aerosol
microphysics model**

Y. H. Lee et al.

[Title Page](#)

[Abstract](#)

[Introduction](#)

[Conclusions](#)

[References](#)

[Tables](#)

[Figures](#)



[Back](#)

[Close](#)

[Full Screen / Esc](#)

[Printer-friendly Version](#)

[Interactive Discussion](#)



Table 1. Summary of TOMAS and the bulk aerosol model processes.

Emission/Process	TOMAS model	Bulk model
Anthropogenic emissions	CMIP5 2000 emissions (Lamarque et al., 2012)	CMIP5 2000 emissions (Lamarque et al., 2012)
Biomass burning emissions	Climatological-average GFED3 emissions from 1997 to 2009 (van der Werf et al., 2010)	Climatological-average GFED3 emissions from 1997 to 2009 (van der Werf et al., 2010)
Primary sulfate emission assumption	1.0 % of total sulfur emissions	2.5 % of total sulfur emissions
DMS emission	Seawater DMS concentrations from Kettle et al. (1999) Sea-to-air transfer function from Liss and Merlivat (1986)	Seawater DMS concentrations from Kettle et al. (1999) Sea-to-air transfer function from Nightingale et al. (2000)
Sea-salt emission	Gong et al. (2002); the upper diameter limit of 10 µm	Gong et al. (2002); the upper diameter limit of 8 µm
Dust emission	See text for the details; the upper size diameter of 10 µm	See text for the details; the upper size diameter of 16 µm
Nucleation	Three nucleation cases 1. BASE – Binary nucleation 2. LowNUC – Binary nucleation with 5 times lower sulfuric acid concentrations 3. NoNUC – no nucleation	N/A

[Title Page](#)[Abstract](#)[Introduction](#)[Conclusions](#)[References](#)[Tables](#)[Figures](#)[◀](#)[▶](#)[◀](#)[▶](#)[Back](#)[Close](#)[Full Screen / Esc](#)[Printer-friendly Version](#)[Interactive Discussion](#)

**ModelE2-TOMAS:
global aerosol
microphysics model**

Y. H. Lee et al.

Table 2. Emission size distributions assumed in TOMAS. ^a This is the soil size assumption used in ModelE2-TOMAS, and the dust emission size distribution is additionally influenced by meteorological variables.

Species	Emissions	Size assumptions
Sulfate	All emissions	Bimodal distribution GMD = 10 nm, GSD = 1.6 (5 % of total mass) GMD = 70 nm, GSD = 2.0 (95 % of total mass)
EC and OC	Fossil fuel and Biofuel Biomass burning	GMD = 60 nm, GSD = 1.59 GMD = 150 nm, GSD = 1.59
Dust ^a	Clay Silt	GMD = 140 nm, GSD = 2.0 GMD = 1.15 µm, GSD = 2.0

[Title Page](#)[Abstract](#)[Introduction](#)[Conclusions](#)[References](#)[Tables](#)[Figures](#)[Back](#)[Close](#)[Full Screen / Esc](#)[Printer-friendly Version](#)[Interactive Discussion](#)

ModelE2-TOMAS:
 global aerosol
 microphysics model

Y. H. Lee et al.

Title Page	
Abstract	Introduction
Conclusions	References
Tables	Figures
◀	▶
◀	▶
Back	Close
Full Screen / Esc	
Printer-friendly Version	
Interactive Discussion	



Table 3. Global budgets for DMS and SO₂ from the BASE run in ModelE2-TOMAS. Values in parentheses are ranges from other global models including Wang et al. (2011), Liu et al. (2005), and those listed in Liu et al. (2005).

	DMS	SO ₂
Burden [Tg S]	0.05 (0.02–0.15)	0.36 (0.2–0.69)
Total source [Tg S yr ⁻¹]	16.1	80
Emission	16.1 (10.7–23.7)	65.6 (61.2–92.0)
Chemistry	—	14.4
Sink [Tg S yr ⁻¹]	16.1	80
Gas-phase oxidation	16.1 (6.1–22.0)	12.3
Aqueous-phase oxidation	— (24.5–57.8)	30.8
Wet deposition	— (0–19.9)	0.36
Dry deposition	— (15.78–55)	37
Lifetime [days]	1.2 (0.5–3.0)	1.9 (0.6–2.6)

Table 4. Global budgets for DMS and SO₂ in the bulk aerosol model.

	DMS	SO ₂
Burden [Tg S]	0.11	0.38
Total source [Tg S yr ⁻¹]	28.7	90
Emission	28.7	64.7
Chemistry	–	25.3
Sink [Tg S yr ⁻¹]	28.7	89
Gas-phase oxidation	28.7	14.6
Aqueous-phase oxidation	–	35.8
Wet deposition	–	0.4
Dry deposition	–	38.8
Lifetime [days]	1.5	1.5

[Title Page](#) [Abstract](#) [Introduction](#) [Conclusions](#) [References](#) [Tables](#) [Figures](#) [◀](#) [▶](#) [◀](#) [▶](#) [Back](#) [Close](#) [Full Screen / Esc](#) [Printer-friendly Version](#) [Interactive Discussion](#)



[Title Page](#)[Abstract](#)[Introduction](#)[Conclusions](#)[References](#)[Tables](#)[Figures](#)[Back](#)[Close](#)[Full Screen / Esc](#)[Printer-friendly Version](#)[Interactive Discussion](#)

Table 5. Global aerosol budgets of the BASE run in ModelE2-TOMAS. Values in the parentheses are the mean and normalized stand deviations obtained from Table 10 in Textor et al. (2006). The mass budgets for sulfate are presented as Tg S.^a For sea-salt emission, the median value from Textor et al. (2006) is presented because the mean value (16 600 Tg yr⁻¹) seems too high.

	Sulfate	Elemental carbon (EC)	Organic matter (OM)	Sea-salt	Dust
Burden [Tg]	0.67 (0.66, 25 %)	0.19 (0.24, 42 %)	1.2 (1.7, 27 %)	3.6 (7.5, 54 %)	9.1 (19, 40 %)
Total source [Tg yr ⁻¹]	43.7 (59.7, 22 %)	7.4 (11.9, 23 %)	60.8 (96.6, 26 %)	3231.9 (6280 ^a , 199 %)	705.8 (1840, 49 %)
Emission	0.66	7.4	43.7	3231.9	705.8
Wet deposition [Tg yr ⁻¹]	42.9	7.1	59.1	1046.9	336.8
By moist convective clouds [%]	27	24	24	54	29
Dry deposition [Tg yr ⁻¹]	0.8	0.3	1.6	2184.9	369.9
Lifetime [days]	5.6 (4.1, 18 %)	9.6 (7.1, 33 %)	7.2 (6.5, 27 %)	0.4 (0.5, 58 %)	4.7 (4.1, 43 %)
Removal rate coefficient [day ⁻¹]	0.18 (0.25, 18 %)	0.10 (0.15, 21 %)	0.14 (0.16, 24 %)	2.4 (5.1, 188 %)	0.21 (0.31, 62 %)
Wet deposition	0.18 (0.22, 22 %)	0.10 (0.12, 31 %)	0.14 (0.14, 32 %)	0.79 (0.79, 77 %)	0.10 (0.08, 42 %)
Dry deposition	0.0032 (0.03, 55 %)	0.004 (0.03, 55 %)	0.0037 (0.03, 49 %)	1.6 (4.3, 219 %)	0.11 (0.23, 84 %)
Wet/(Wet +Dry) [%]	98 (89, 8 %)	96 (79, 17 %)	97 (80, 16 %)	32 (31, 65 %)	48 (33, 54 %)

Table 6. Global aerosol budgets in the bulk aerosol model. Note that the sulfate and nitrate budgets are presented as Tg S and Tg N, respectively.

	Sulfate	EC	OM	Sea-salt	Dust	Nitrate
Burden [Tg]	0.38	0.12	1.1	9.3	11.4	0.37
Total source [Tg yr ⁻¹]	52.0	7.4	58.5	2866.7	1071.8	21.0
Emission	1.7	7.4	43.7	2866.7	1071.8	
Wet deposition [Tg yr ⁻¹]	46.6	5.4	44.9	2059.1	407.7	17.7
By moist convective clouds [%]	21	37	32	39	52	29
Dry deposition [Tg yr ⁻¹]	5.4	2.0	13.7	806.9	664.1	3.3
Lifetime [days]	2.6	5.8	7.1	1.2	3.9	6.4
Removal rate coefficient [day ⁻¹]	0.39	0.17	0.14	0.84	0.26	0.16
Wet deposition	0.35	0.13	0.11	0.61	0.10	0.13
Dry deposition	0.04	0.046	0.033	0.24	0.16	0.025
Wet/(Wet +Dry) [%]	90	73	77	72	38	84



**ModelE2-TOMAS:
global aerosol
microphysics model**

Y. H. Lee et al.

Table 7. Statistical measures of model predictions compared to satellites. For the bulk aerosol model, the model prediction without nitrate aerosols is also presented in parentheses.

		Model vs. MODIS	Model vs. MISR	MODIS vs. MISR
TOMAS	Correlation	0.63	0.73	0.79
	NMB [%]	-29 %	-34 %	8 %
Bulk aerosol model	Correlation	0.45 (0.45)	0.52 (0.55)	0.79
	NMB [%]	16 % (-16 %)	8 % (-21 %)	8 %

- [Title Page](#)
- [Abstract](#) [Introduction](#)
- [Conclusions](#) [References](#)
- [Tables](#) [Figures](#)
- [◀](#) [▶](#)
- [◀](#) [▶](#)
- [Back](#) [Close](#)
- [Full Screen / Esc](#)
- [Printer-friendly Version](#)
- [Interactive Discussion](#)



ModelE2-TOMAS:
global aerosol
microphysics model

Y. H. Lee et al.

[Title Page](#)[Abstract](#)[Introduction](#)[Conclusions](#)[References](#)[Tables](#)[Figures](#)

Back

Close

[Full Screen / Esc](#)[Printer-friendly Version](#)[Interactive Discussion](#)

	Sites	Longitude	Latitude	Years
1	Alta Floresta	56.0° W	9.9° S	1999–2005
2	Abracos Hill	62.0° W	11° S	1999–2005
3	Cuiaba-Miranda	56.0° W	15.7° S	2001–2005
4	Mongu	23.2° E	15.2° S	1995–2005
5	Ilorin	4.3° E	8.3° N	1998–2005
6	Banizombou	2.0° E	13.0° N	1995–2005
7	Capo Verde	22.9° W	16.7° N	1994–2004
8	Bidi Bahn	2.5° W	14.1° N	1996–1997
9	Barbados	59.5° W	13.2° N	1996–2000
10	Sede Boker	34.8° E	30.9° N	1998–2005
11	Bahrain	50.6° E	26.2° N	2004–2005
12	Solar Village	46.4° E	24.9° N	1999–2005
13	Dalanzadgad	104.4° E	43.6° N	1997–2005
14	Yulin	109.7° E	38.3° N	2001–2002
15	Sevilleta	106.9° W	34.4° N	1994–2005
16	Cart site	97.5° W	36.6° N	1996–2005
17	Bondville	88.4° W	40.1° N	1996–2005
18	GSFC	76.8° W	39.0° N	1995–2005
19	Mexico city	99.2° W	19.3° N	1999–2005
20	Ispra	8.6° E	45.8° N	2001–2005
21	Kanpur	80.3° E	26.5° N	2001–2005
22	Shirahama	135.4° E	33.7° N	2000–2005
23	Bermuda	64.7° W	32.4° N	1996–2005
24	Lanai	156.9° W	20.7° N	1996–2004
25	Dry Tortugas	82.9° W	24.6° N	1996–2003
26	Tahiti	149.6° W	17.6° S	1999–2005
27	Rottnest Island	115.5° E	32.0° N	2001–2004
28	Nauru	166.9° E	0.5° S	1999–2005

ModelE2-TOMAS: global aerosol microphysics model

Y. H. Lee et al.

Table 9. Summary of global annual-average of tropospheric and surface-layer aerosol number budgets including J3 (new particle formation rates at 3 nm), CN3 (number concentration of particles with $D_p \geq 3$ nm), CN10 ($D_p \geq 10$ nm), CN100 ($D_p \geq 100$ nm) in ModelE2-TOMAS. Values normalized by tropospheric volume at 273 K and 1 atm.

	Emission rate [cm ⁻³ s ⁻¹]	Tropo-spheric J3 [cm ⁻³ s ⁻¹]	Tropo-spheric CN3 [cm ⁻³]	Tropo-spheric CN10 [cm ⁻³]	Tropo-spheric CN100 [cm ⁻³]	Surface-layer CN3 [cm ⁻³]	Surface-layer CN10 [cm ⁻³]	Surface-layer CN100 [cm ⁻³]
Base	5.47×10^{-4}	0.131	4852	939	211	1622	1331	416
LowNUC	5.47×10^{-4}	0.013	1277	628	197	1152	1111	405
NoNUC	5.47×10^{-4}	0.000	222	221	159	935	919	374

- [Title Page](#)
- [Abstract](#) [Introduction](#)
- [Conclusions](#) [References](#)
- [Tables](#) [Figures](#)
- [◀](#) [▶](#)
- [◀](#) [▶](#)
- [Back](#) [Close](#)
- [Full Screen / Esc](#)
- [Printer-friendly Version](#)
- [Interactive Discussion](#)



**ModelE2-TOMAS:
global aerosol
microphysics model**

Y. H. Lee et al.

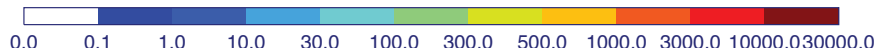
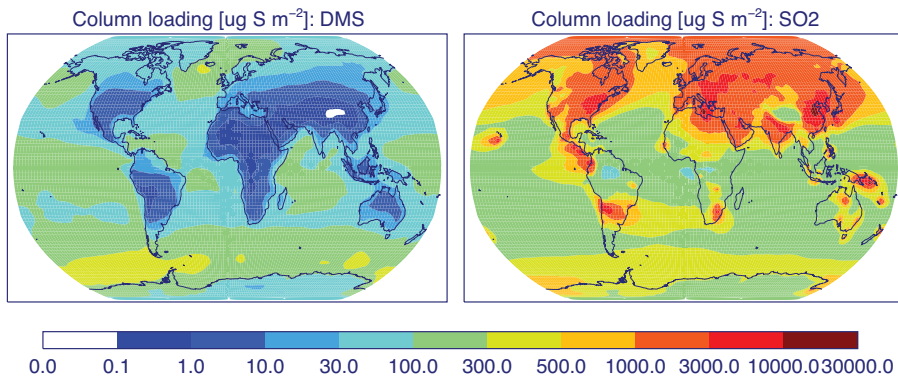


Figure 1. Annual-average DMS and SO_2 column mass concentrations in the ModelE2-TOMAS BASE run. Units are $\mu\text{g S m}^{-2}$.

- [Title Page](#)
- [Abstract](#) [Introduction](#)
- [Conclusions](#) [References](#)
- [Tables](#) [Figures](#)
- [◀](#) [▶](#)
- [◀](#) [▶](#)
- [Back](#) [Close](#)
- [Full Screen / Esc](#)
- [Printer-friendly Version](#)
- [Interactive Discussion](#)



**ModelE2-TOMAS:
global aerosol
microphysics model**

Y. H. Lee et al.

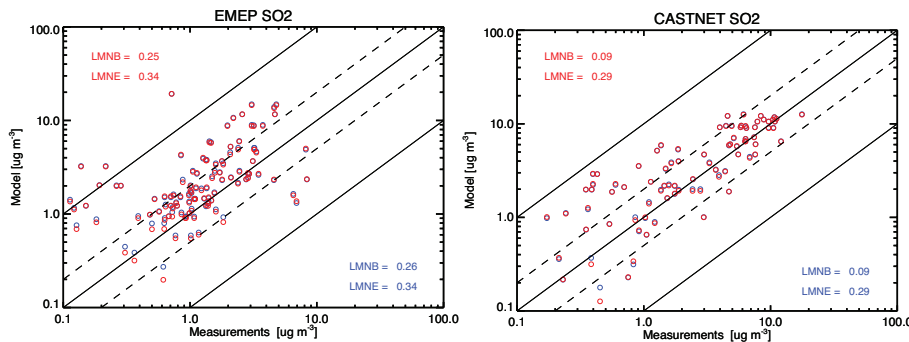


Figure 2. Scatter plot of annual-mean surface SO₂ concentrations [$\mu\text{g m}^{-3}$] for the model (red for the TOMAS model and blue for the bulk aerosol model) compared to the observations in the EMEP (European Monitoring and Evaluation Programme, Loeblad et al., 2004) and CASTNET (Clean Air Status and Trends Network, Malm et al., 2002) networks. Log-mean normalized bias (LMNB) and log-mean normalized error (LMNE) are given.

[Title Page](#)
[Abstract](#) [Introduction](#)
[Conclusions](#) [References](#)
[Tables](#) [Figures](#)

[◀](#) [▶](#)
[◀](#) [▶](#)
[Back](#) [Close](#)
[Full Screen / Esc](#)
[Printer-friendly Version](#)
[Interactive Discussion](#)



ModelE2-TOMAS: global aerosol microphysics model

Y. H. Lee et al.

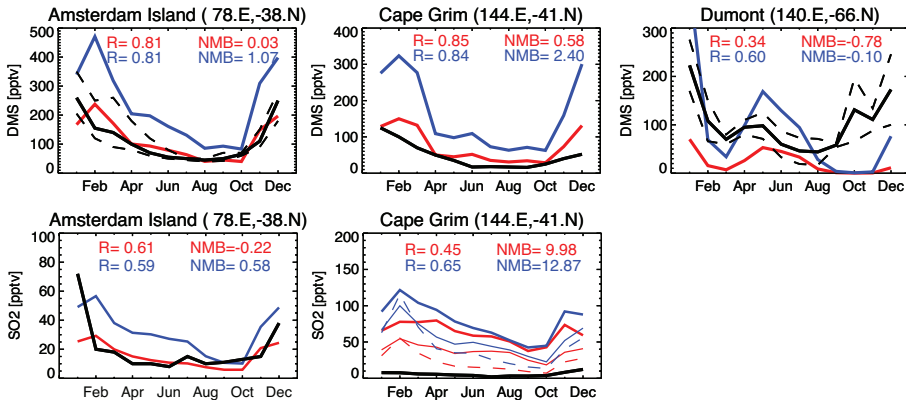


Figure 3. Comparisons of monthly averaged surface SO₂ and DMS mixing ratios [pptv] simulated (red for the TOMAS model and blue for the bulk aerosol model) and measured (black) at Amsterdam Island (Nguyen et al., 1992) and Cape Grim (Ayers et al., 1991). Only DMS at Dumont D'Urville (Jourdain and Legrand, 2001). Correlation (*R*) and normalized mean bias (NMB) are given.

- [Title Page](#)
- [Abstract](#) [Introduction](#)
- [Conclusions](#) [References](#)
- [Tables](#) [Figures](#)
- [◀](#) [▶](#)
- [◀](#) [▶](#)
- [Back](#) [Close](#)
- [Full Screen / Esc](#)
- [Printer-friendly Version](#)
- [Interactive Discussion](#)



ModelE2-TOMAS: global aerosol microphysics model

Y. H. Lee et al.

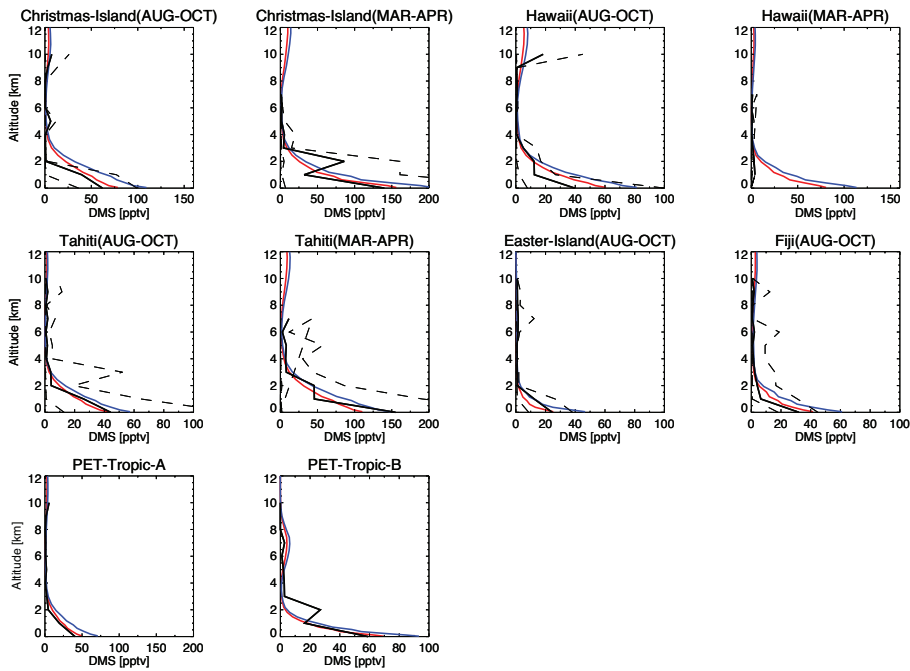


Figure 4. Comparison of DMS vertical profiles over the Pacific Ocean simulated (red for the TOMAS model and blue for the bulk aerosol model) and observed (black solid line). Observations are from PEM-Tropic-A (August–October 1996 in the tropical Pacific) and PEM-Tropic-B (March–April 1999 in the tropical Pacific). The dashed lines represent 25th and 75th percentiles of the observed values.

ModelE2-TOMAS: global aerosol microphysics model

Y. H. Lee et al.

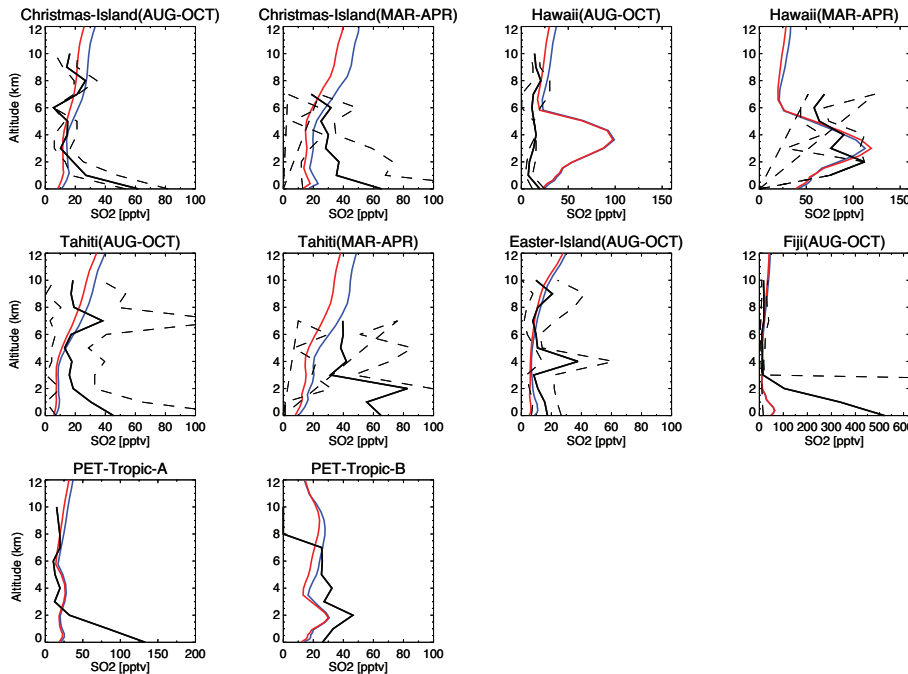


Figure 5. The same as Fig. 4 but for SO₂ vertical profiles.

**ModelE2-TOMAS:
global aerosol
microphysics model**

Y. H. Lee et al.

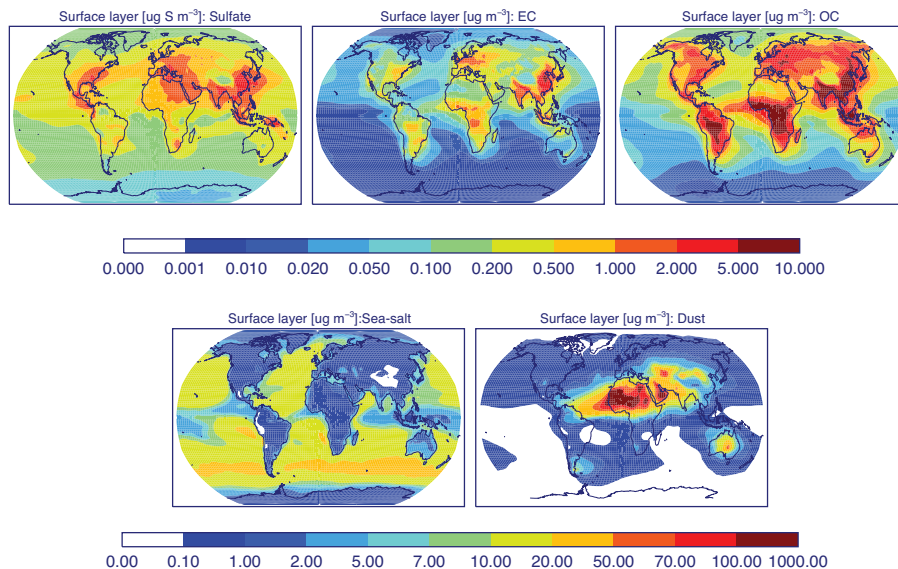


Figure 6. Annual-mean sulfate, EC, OM, sea-salt, and dust concentrations in the lowermost layer in the ModelE2-TOMAS BASE run. Units are $\mu\text{g S m}^{-3}$ for sulfate, $\mu\text{g m}^{-3}$ for the rest.

**ModelE2-TOMAS:
global aerosol
microphysics model**

Y. H. Lee et al.

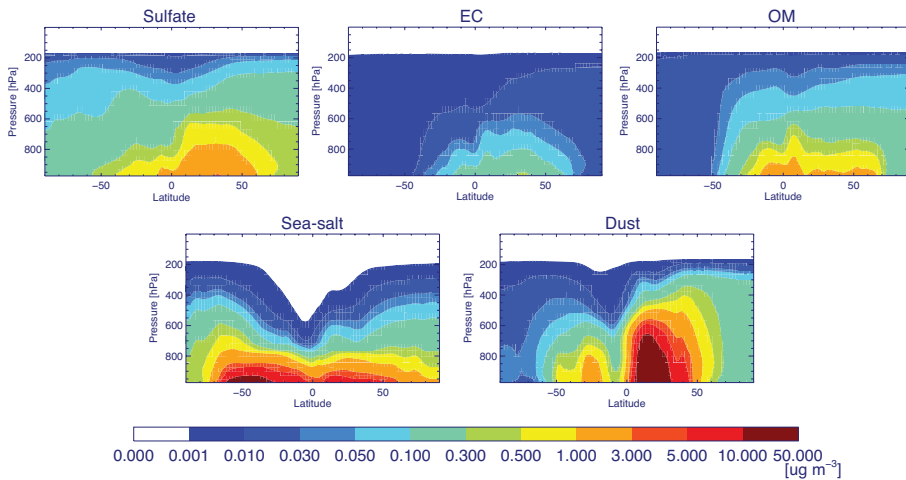


Figure 7. Annually and zonally averaged sulfate, EC, OM, sea-salt, and dust concentrations of the BASE run in the ModelE2-TOMAS. Units are $\mu\text{g m}^{-3}$.

[Title Page](#)[Abstract](#)[Introduction](#)[Conclusions](#)[References](#)[Tables](#)[Figures](#)[Back](#)[Close](#)[Full Screen / Esc](#)[Printer-friendly Version](#)[Interactive Discussion](#)

**ModelE2-TOMAS:
global aerosol
microphysics model**

Y. H. Lee et al.

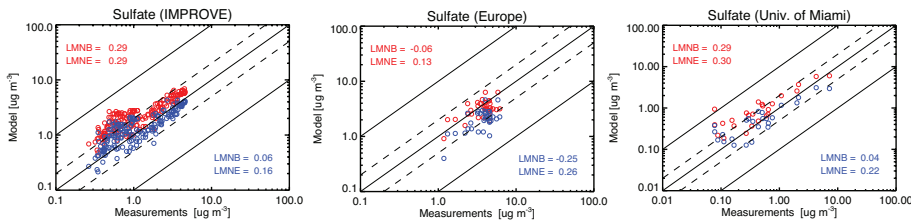


Figure 8. Scatter plot of annually averaged surface sulfate mass concentrations [$\mu\text{g m}^{-3}$] in the model (red for the TOMAS model and blue for the bulk aerosol model) and observation from the IMPROVE network, the European sites from Putaud et al. (2010), and University of Miami. Note that the sulfate in the model is simply converted to ammonium sulfate at the IMPROVE sites.

ModelE2-TOMAS: global aerosol microphysics model

Y. H. Lee et al.

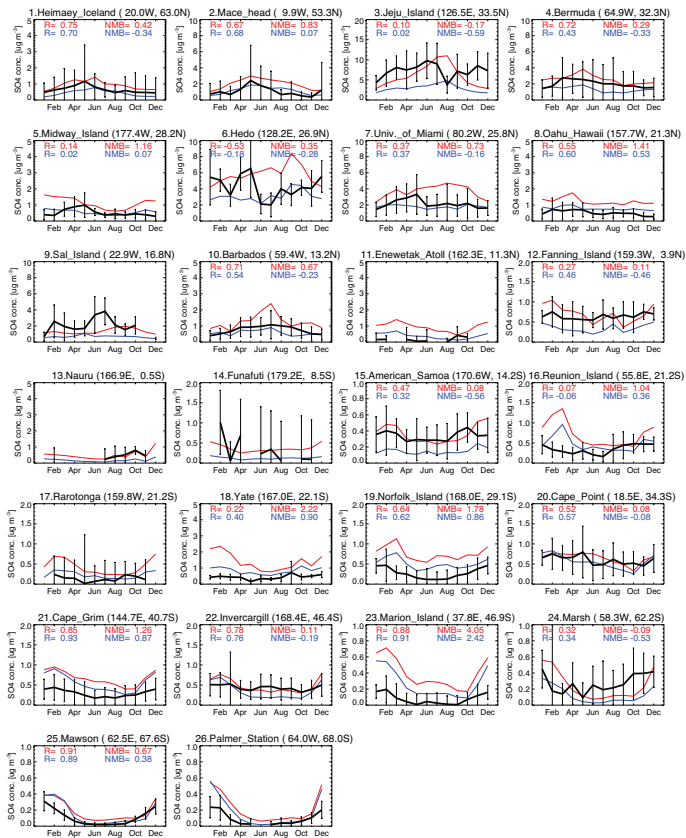


Figure 9. Comparisons of monthly averaged surface sulfate mass concentrations [$\mu\text{g m}^{-3}$] simulated (red for the TOMAS model and blue for the bulk aerosol model) and measured (black solid line with an error bar showing a standard deviation) by University of Miami. Correlation (R) and normalized mean bias (NMB) are provided only when the observation is available for 12 months.

ModelE2-TOMAS: global aerosol microphysics model

Y. H. Lee et al.

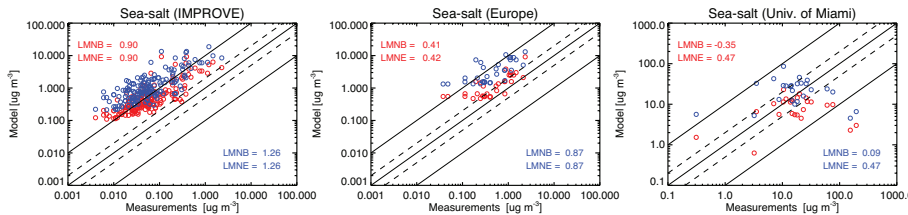


Figure 10. Same as Fig. 8 but for sea-salt mass concentrations.

Title Page	
Abstract	Introduction
Conclusions	References
Tables	Figures

◀	▶
◀	▶
Back	Close
Full Screen / Esc	

Printer-friendly Version
Interactive Discussion



ModelE2-TOMAS: global aerosol microphysics model

Y. H. Lee et al.

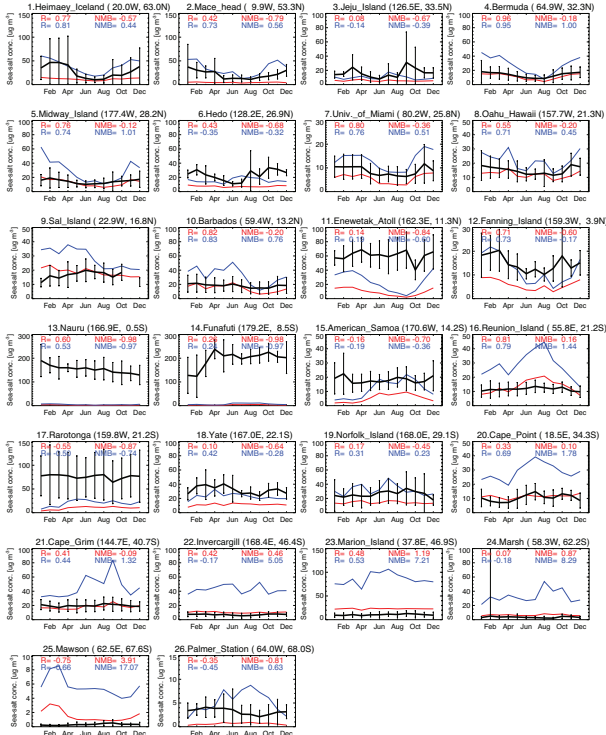


Figure 11. Comparisons of monthly averaged surface sea-salt mass concentrations [$\mu\text{g m}^{-3}$] simulated (red for the TOMAS model and blue for the bulk aerosol model) and measured (black solid line with an error bar showing a standard deviation) by University of Miami. Correlation (R) and normalized mean bias (NMB) are provided only when the observation is available for 12 months.



**ModelE2-TOMAS:
global aerosol
microphysics model**

Y. H. Lee et al.

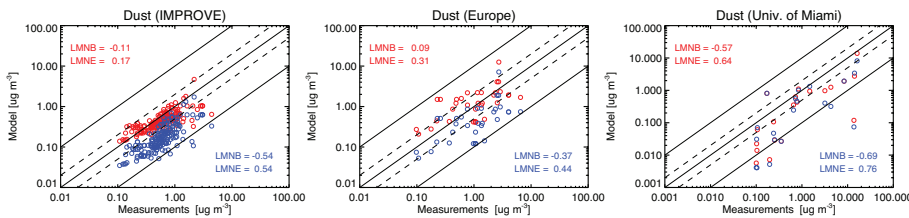


Figure 12. Same as Fig. 8 but for dust mass concentrations.

**ModelE2-TOMAS:
global aerosol
microphysics model**

Y. H. Lee et al.

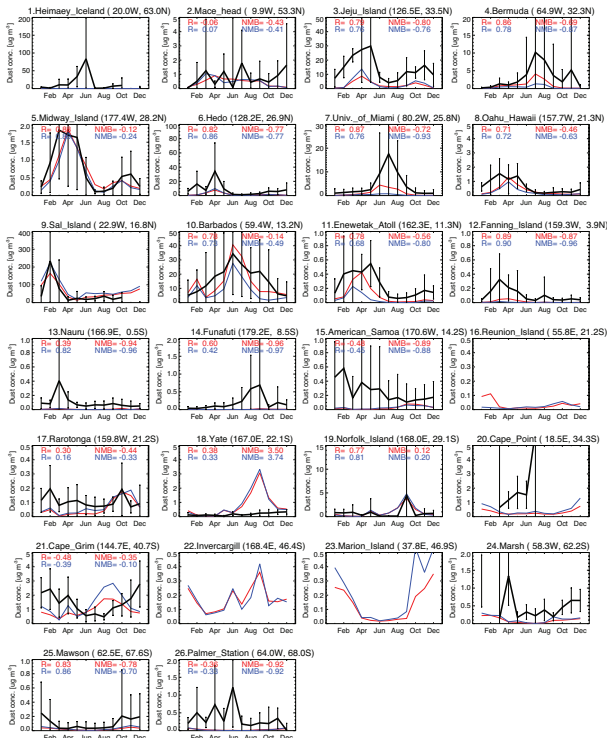
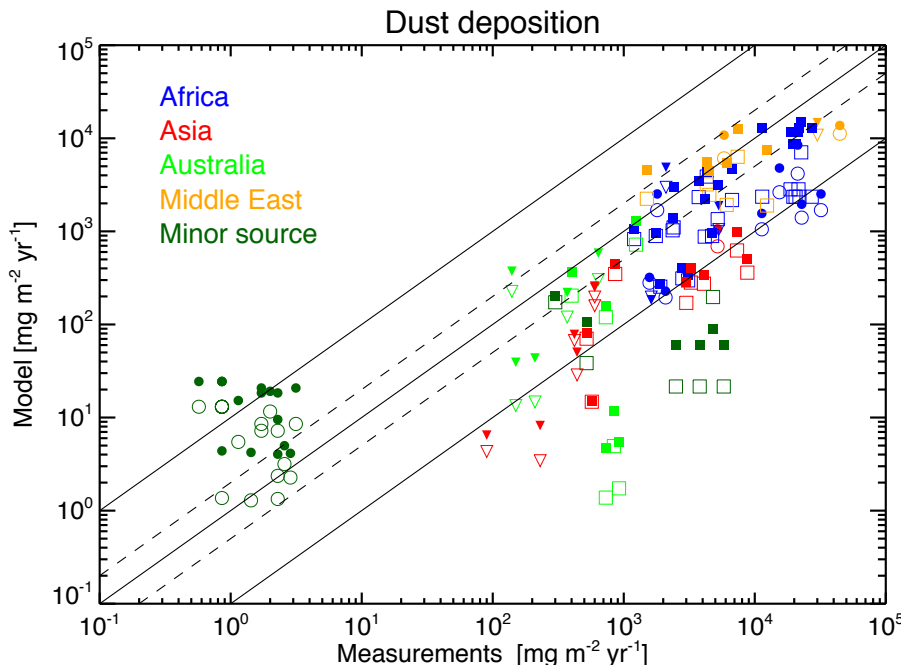


Figure 13. Comparisons of monthly averaged surface dust mass concentrations [$\mu\text{g m}^{-3}$] simulated (red for the TOMAS model and blue for the bulk aerosol model) and measured (black solid line with an error bar showing a standard deviation) by University of Miami. Correlation coefficient (R) and normalized mean bias (NMB) are provided only when observations are available for 12 months.

ModelE2-TOMAS: global aerosol microphysics model

Y. H. Lee et al.



Mahowald et al.[2009] - o

LMNB = -0.04

LMNE = 0.68

LMNB = 0.24

LMNE = 0.82

Ginoux et al.[2001] - v

LMNB = -0.77

LMNE = 0.81

LMNB = -0.54

LMNE = 0.64

Tegen et al.[2002] - sq

LMNB = -0.90

LMNE = 0.91

LMNB = -0.61

LMNE = 0.65

Figure 14. Scatter plot of annual-average dust deposition fluxes [$\text{mg m}^{-2} \text{yr}^{-1}$] simulated and observations obtained from Ginoux et al. (2001), Tegen et al. (2002) and Tables S2 in Mahowald et al. (2009). Open symbols are for the TOMAS model and the filled symbol for the bulk aerosol model. LMNB and LMNE are presented below the plot: the first values are for TOMAS.

ModelE2-TOMAS: global aerosol microphysics model

Y. H. Lee et al.

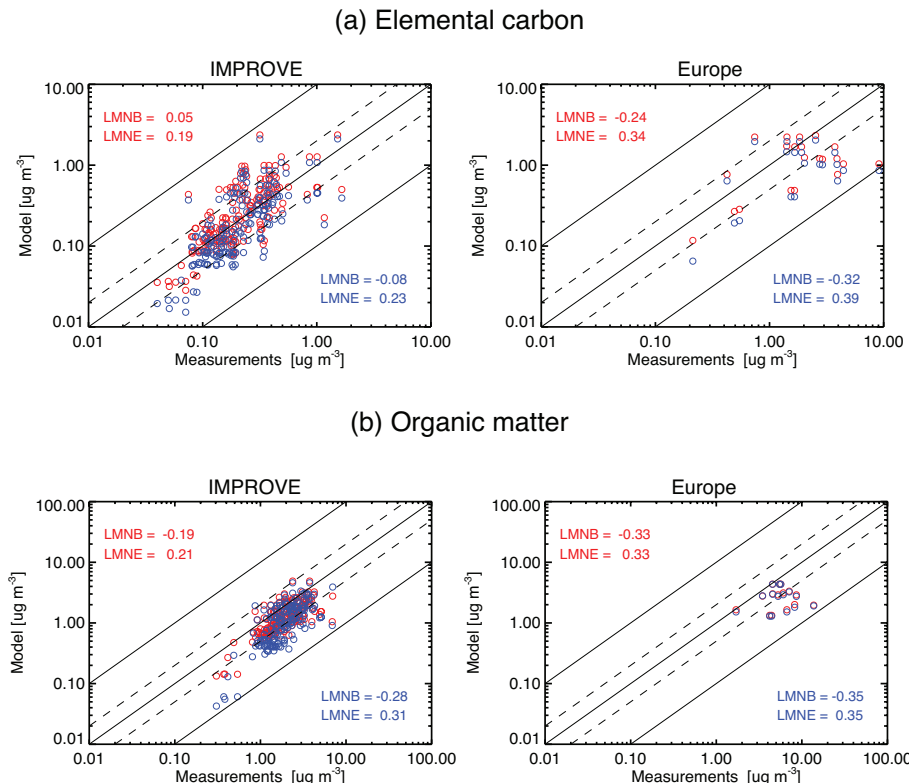


Figure 15. Scatter plot of annually averaged surface mass concentrations [$\mu\text{g m}^{-3}$] of (a) elemental carbon and (b) organic matter simulated (red for the TOMAS model and blue for the bulk aerosol model) and observed in the IMPROVE network and the European sites from Putaud et al. (2010).

ModelE2-TOMAS: global aerosol microphysics model

Y. H. Lee et al.

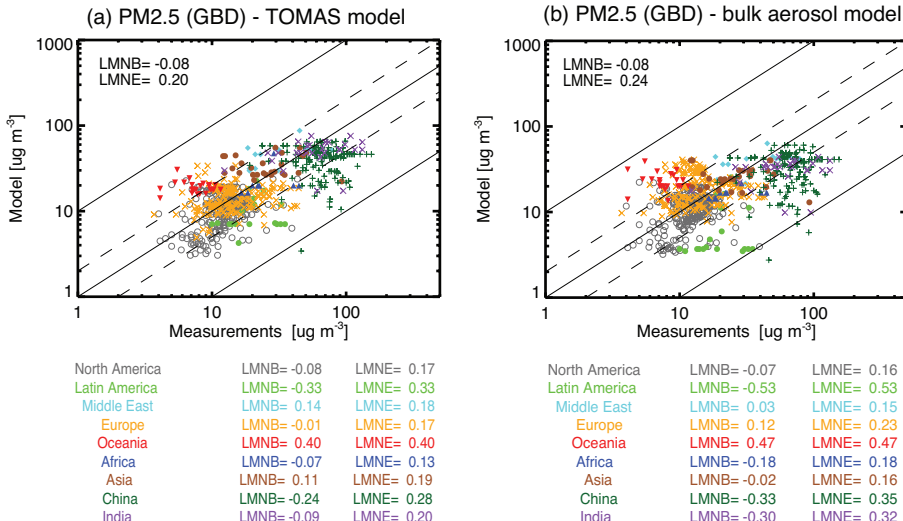


Figure 16. Scatter plot of annually averaged surface PM_{2.5} concentration [$\mu\text{g m}^{-3}$] predictions and observations compiled by the Global Burden of Disease (GBD) Study. TOMAS is shown in (a) and the bulk model in (b).

Title Page

Abstract

Introduction

Conclusions

References

Tables

Figures



Back

Close

Full Screen / Esc

[Printer-friendly Version](#)

Interactive Discussion



**ModelE2-TOMAS:
global aerosol
microphysics model**

Y. H. Lee et al.

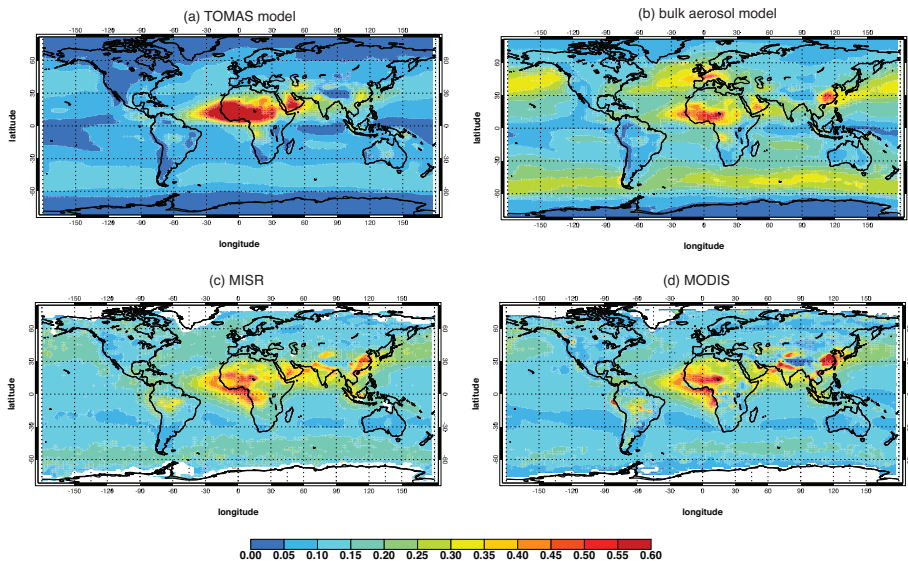


Figure 17. Global distributions of the annual-mean AOD from **(a)** the TOMAS model, **(b)** the bulk aerosol model, **(c)** MISR, and **(d)** MODIS. See Sect. 5.4 for the details of the MISR and MODIS AOD information.

[Title Page](#)[Abstract](#)[Introduction](#)[Conclusions](#)[References](#)[Tables](#)[Figures](#)[Back](#)[Close](#)[Full Screen / Esc](#)[Printer-friendly Version](#)[Interactive Discussion](#)

ModelE2-TOMAS: global aerosol microphysics model

Y. H. Lee et al.

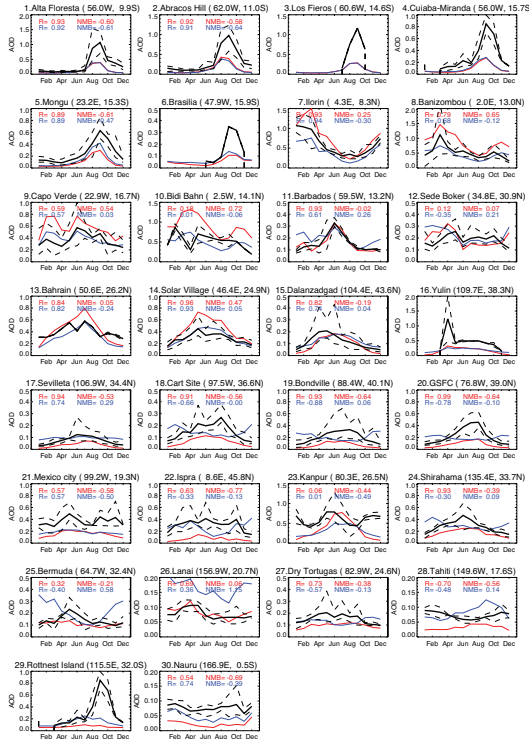


Figure 18. Comparisons of monthly averaged model AOD (red for the TOMAS model and blue for the bulk aerosol model) and AERONET AOD (black solid line). Correlation (R) and normalized mean bias (nmb) are provided only when the observation is available for 12 months.



ModelE2-TOMAS: global aerosol microphysics model

Y. H. Lee et al.

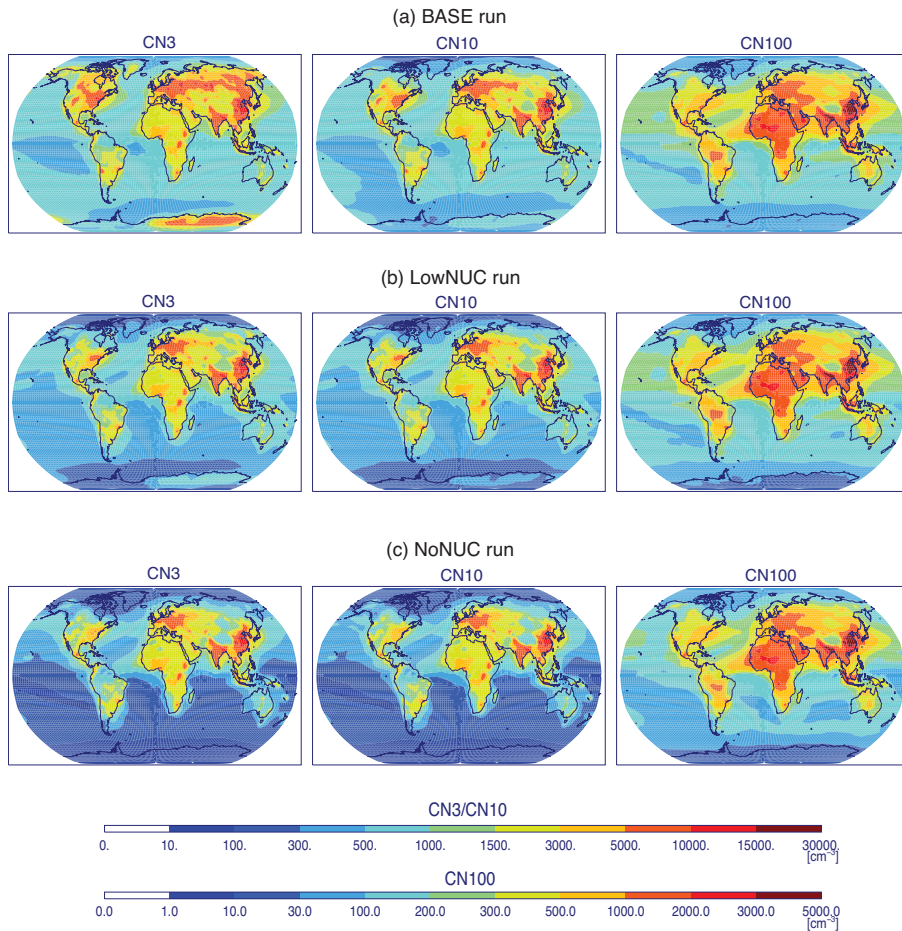


Figure 19. Annually averaged CN3 ($D_p \geq 3\text{ nm}$), CN10 ($D_p \geq 10\text{ nm}$), CN100 ($D_p \geq 100\text{ nm}$) concentrations in the lowermost layer. Units are cm^{-3} .

ModelE2-TOMAS: global aerosol microphysics model

Y. H. Lee et al.

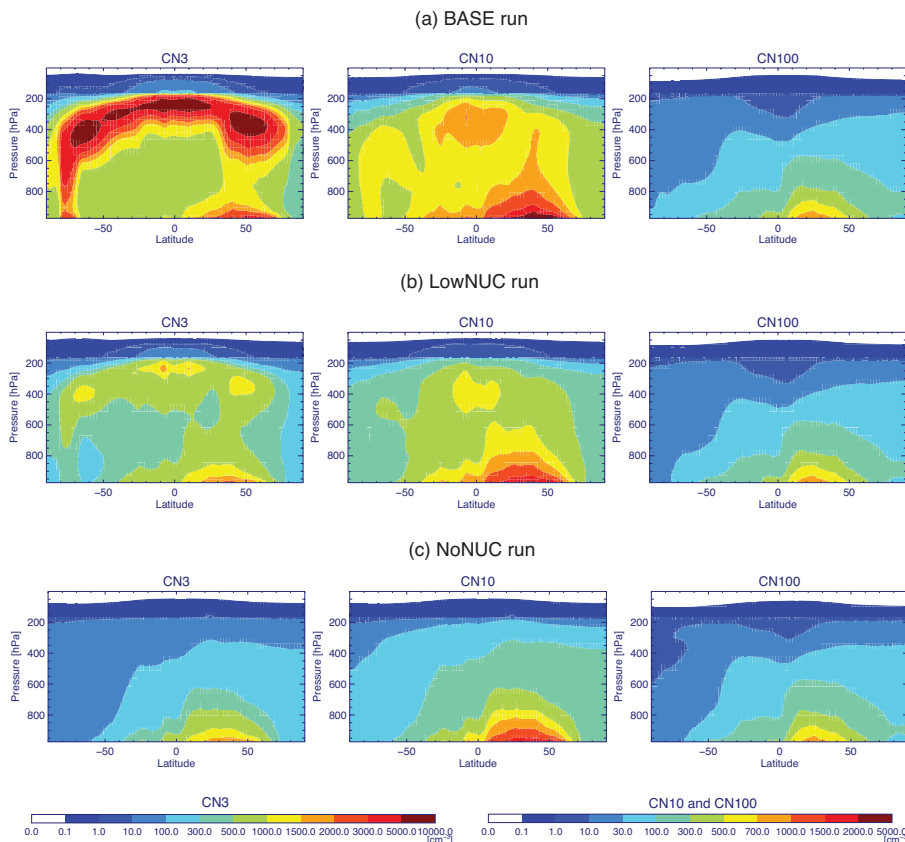


Figure 20. Annually and zonally averaged CN3 ($D_p \geq 3 \text{ nm}$), CN10 ($D_p \geq 10 \text{ nm}$), and CN100 ($D_p \geq 100 \text{ nm}$) concentrations. Units are cm^{-3} .

**ModelE2-TOMAS:
global aerosol
microphysics model**

Y. H. Lee et al.

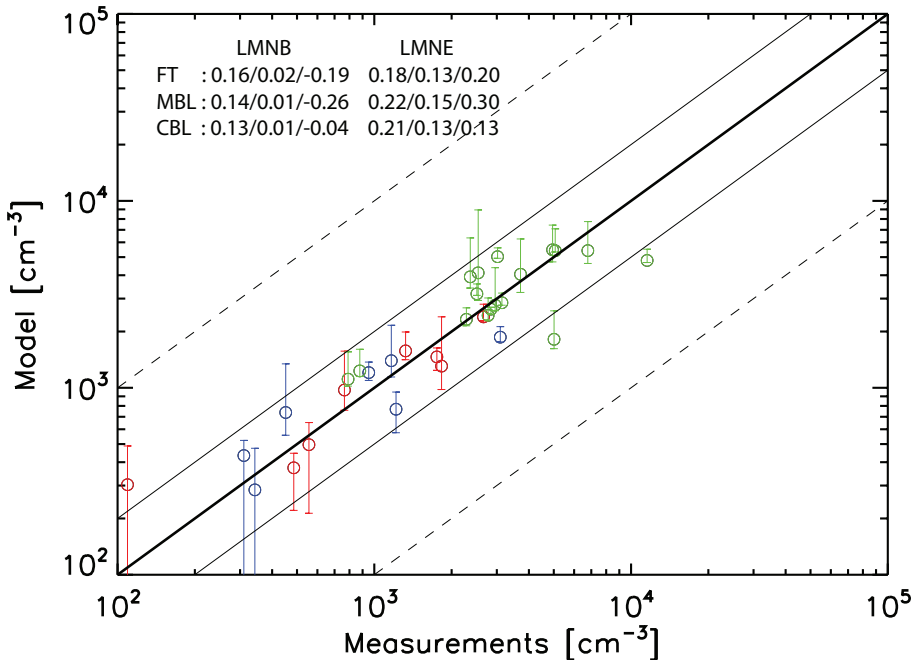


Figure 21. Scatter plot of simulated annual-mean aerosol number concentrations in comparison with a dataset of surface number concentrations measurements at 36 sites around the world compiled by Spracklen et al. (2010). The circle symbols represent the LowNUC results, and the upper error bar the BASE results and the lower error bar the NoNUC results. Red color is for free troposphere (FT); blue for marine boundary layer (MBL); green for continental boundary layer (CBL). LMNB and LMNB are shown in the following order: BASE/LowNUC/NoNUC runs.

ModelE2-TOMAS: global aerosol microphysics model

Y. H. Lee et al.

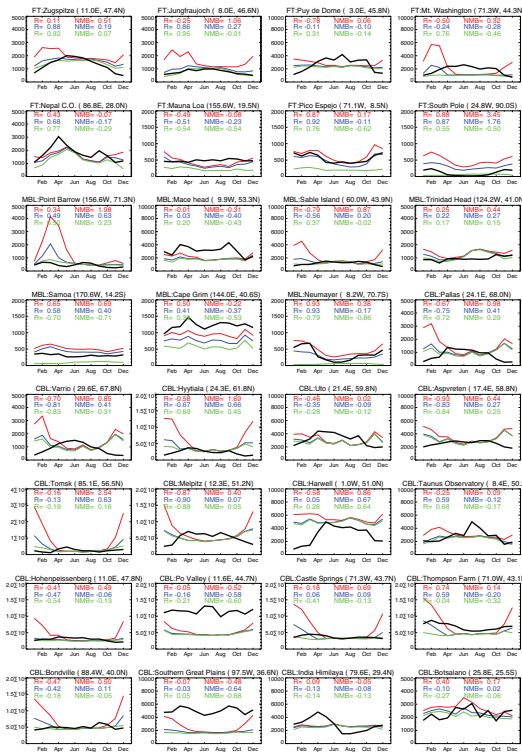


Figure 22. Annual cycle of aerosol number concentrations (cm^{-3} at ambient conditions) at 32 sites. The observations are shown in black, and three model results are presented: red for BASE, blue for LowNUC, and green for NoNUC. The free tropospheric (FT) sites are from Zugspitze to South Pole, and the marine boundary layer (MBL) sites are from Point Barrow to Neumayer, and the continental boundary layer (CBL) sites are from Pallas to Botsalano. Correlation (R) and normalized mean bias (NMB) are provided only when the observation is available for 12 months.

ModelE2-TOMAS: global aerosol microphysics model

Y. H. Lee et al.

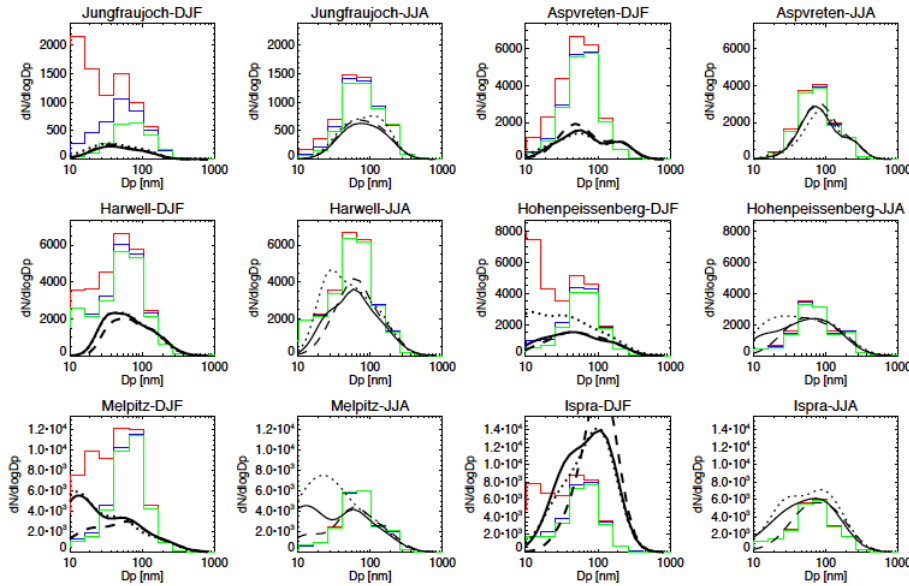


Figure 23. Number size distributions from European sites during winter (DJF) and summer (JJA) that are obtained from log-normal 3-mode fits during morning (black solid), afternoon (black dotted), and night (black dashed). The model results are the seasonal mean, shown in red lines for the BASE run, blue lines for the LowNUC run, and green lines for the NoNUC run.

ModelE2-TOMAS: global aerosol microphysics model

Y. H. Lee et al.

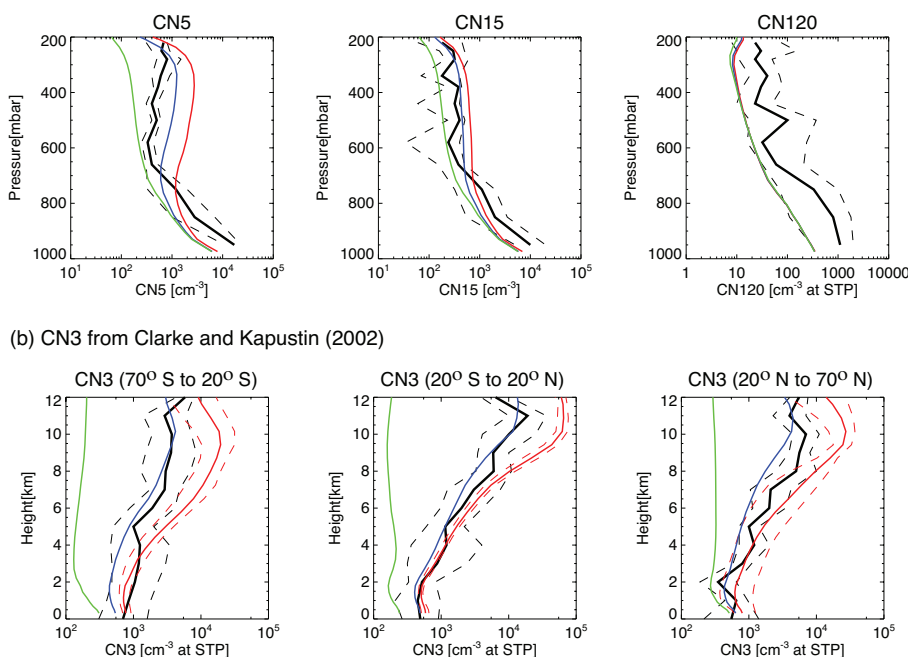


Figure 24. Vertical profiles of aerosol number concentrations from the observations (black lines) and ModelE2-TOMAS (red lines for the BASE run, blue lines for the LowNUC run, and green lines for the NoNUC run). **(a)** Uses CN5, CN15, CN120 concentrations (ambient conditions) from LACE campaign (Petzold et al., 2002, in north-east Germany). **(b)** Uses CN3 concentrations (STP conditions: 1 atm, 273 K) obtained from the various measurements over the Pacific Ocean that are averaged into the 3 latitude bands (70° S to 20° S, 20° S to 20° N, and 20° N to 70° N) (Clarke and Kapustin, 2002). The dashed lines show the standard deviation for the observations and the min/max monthly mean for the model (only in **b**).

Title Page

Abstract

Introduction

Conclusions

References

Tables

Figures



Back

Close

Full Screen / Esc

[Printer-friendly Version](#)

Interactive Discussion

**ModelE2-TOMAS:
global aerosol
microphysics model**

Y. H. Lee et al.

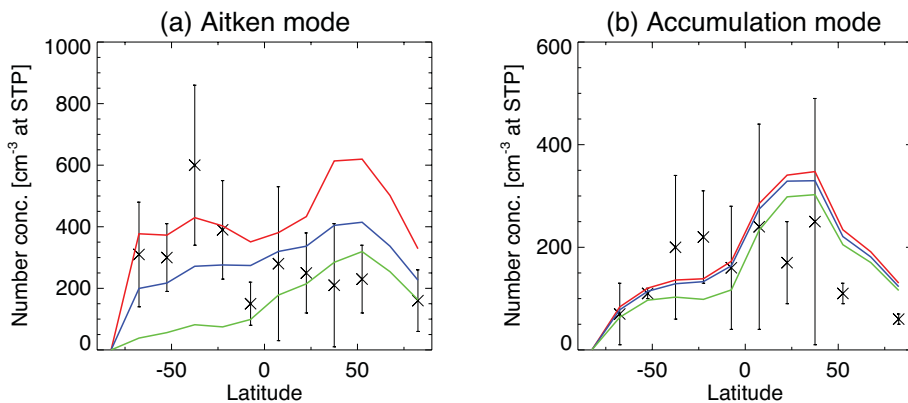


Figure 25. Simulated number concentrations in **(a)** Aitken mode ($10 \text{ nm} \leq D_p < 100 \text{ nm}$) and **(b)** accumulation mode ($100 \text{ nm} \leq D_p < 1 \mu\text{m}$) compared to the observations ("x" symbol with error bar representing minimum and maximum observed concentrations) that were compiled and aggregated into 15° latitude ranges (Heintzenberg et al., 2002). The model is also averaged to the 15° grid and is shown in red lines for the BASE run, blue lines for the LowNUC run, and green lines for the NoNUC run.

[Title Page](#)
[Abstract](#) [Introduction](#)
[Conclusions](#) [References](#)
[Tables](#) [Figures](#)

[◀](#) [▶](#)
[◀](#) [▶](#)

[Back](#) [Close](#)
[Full Screen / Esc](#)

[Printer-friendly Version](#)
[Interactive Discussion](#)

**ModelE2-TOMAS:
global aerosol
microphysics model**

Y. H. Lee et al.

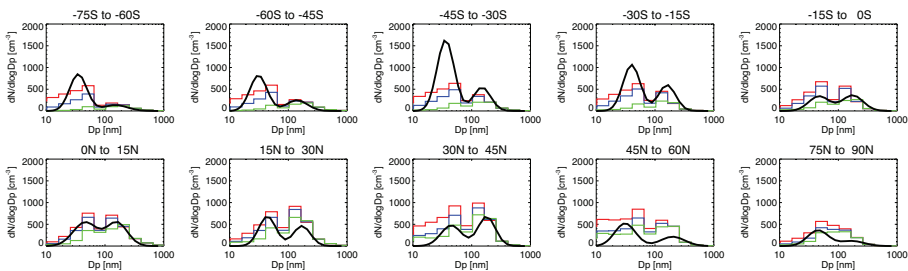


Figure 26. Annually and zonally averaged aerosol size distributions in the marine boundary layer. Observations are from Heintzenberg et al. (2000) and were compiled and aggregated into a $15^\circ \times 15^\circ$ grid. The model is also averaged to the 15° grid and is shown as red lines for the BASE run, blue lines for the LowNUC run, and green lines for the NoNUC run.

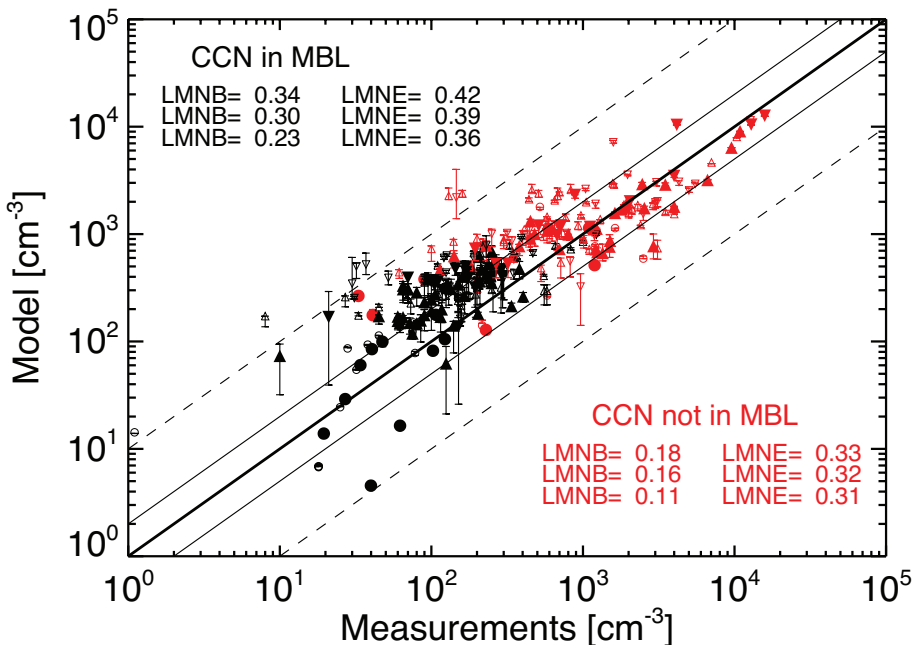


Figure 27. Scatter plot of simulated CCN concentrations in comparison with a dataset of CCN measurements compiled by Spracklen et al. (2011). Data is classified into two categories: CCN in MBL (in black) and CCN not in MBL (in red). The upper error bar is for the BASE run, the middle symbol for the LowNUC run, and the lower error bar for the NoNUC run. Large and filled symbols are for measurement duration longer than 10 days, and small and open symbols for less than 10 days. Circle symbols are for supersaturations (s) less than 0.2 %; upward triangles for s greater than 0.2 % and less than 0.8 %; downward triangle for s greater than 0.8 %.

ModelE2-TOMAS: global aerosol microphysics model

Y. H. Lee et al.

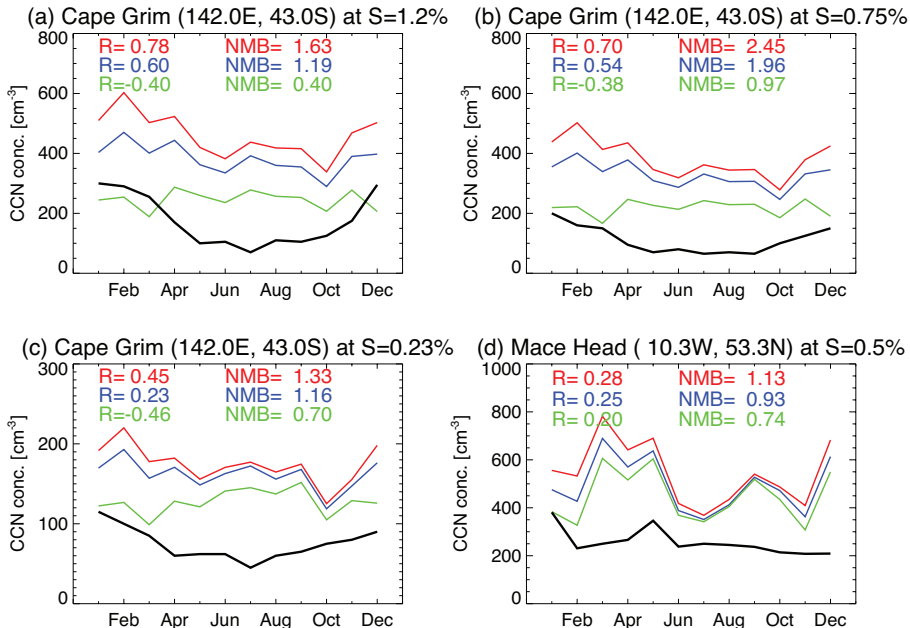


Figure 28. Annual cycle of CCN concentrations at Cape Grim (supersaturations (s) of 1.2% in **a**, 0.75% in **b**, and 0.23% in **c**) and Mace Head (s of 0.5% in **d**). The measured CCN concentrations are shown in black, and the simulated CCN in red for the BASE run, blue for the LowNUC run, and green for the NoNUC run. Correlation (R) and normalized mean bias (NMB) are given.

Title Page

Abstract

Introduction

Conclusio

References

Tables

Figures



Back

Close

Full Screen / Esc

[Printer-friendly Version](#)

Interactive Discussion

